Simulation of the Present-Day Atmospheric Ozone, Odd Nitrogen, Chlorine and Other Species Using a Coupled 2-D Model in Isentropic Coordinates

H. YANG, E. OLAGUER AND K. K. TUNG

Department of Applied Mathematics, University of Washington, Seattle, Washington

(Manuscript received 1 December 1989, in final form 13 August 1990)

ABSTRACT

This paper documents our two-dimensional model which incorporates comprehensive radiative transfer and chemistry modules coupled with self-consistent dynamical transports.

A simultaneous simulation of a range of chemical trace gas species with different photochemical time scales, latitudinal and vertical gradients, and with tropospheric or stratospheric sources is attempted and the result compared with available satellite and in situ observations.

The 2-D model utilizes all zonally averaged physical equations of momentum, energy and mass, and self-consistently determines both its advective and diffusive transport parameters from the observed temperature specific to the period of observation. A major assumption in the formulation is that diffusive mixing is caused by large-scale planetary waves which act predominantly along isentropic surfaces. It is also assumed that it is planetary waves that drive the stratosphere away from radiative equilibrium, resulting in diabatic vertical and meridional advective transport. It is in this way that energy, momentum and tracer budgets are interconnected.

Family approximation is used and the transported species include O_x, NO_y, N_2O, Cl_y, CH_4, CO, CFCs and HF. Partition within a family is calculated assuming photochemical equilibrium. Diurnal variation of nitrogen species is obtained by solving an ordinary differential equation analytically.

The comparison of the model result with observations is very favorable. Some previously known common model deficiencies have largely been overcome. Simulation of climatological ozone, including the details of seasonal, latitudinal and vertical distributions, is especially successful using the present coupled model. The problem of NO_y deficit in the equatorial lower stratosphere also appears to have been resolved, and a correct latitudinal profile for nitric acid column is obtained.

We give physical reasons for the improvements in the model results and discuss possible explanations for the remaining systematic deficiencies, now occurring mostly in the model upper stratosphere and mesosphere, where breaking gravity waves may become an important transport process.

1. Introduction

A *coupled* model for chemical species in the stratosphere is one where feedbacks between dynamical transport, radiative transfer and chemistry are incorporated in the calculation of the chemical composition of the stratosphere. For example, changes in ozone chemistry affecting ozone abundance can alter the radiative properties of the atmosphere, which in turn alter the dynamical transport of ozone itself. The predicted ozone amount should be a result of competing influences of chemistry, dynamics and radiation, and these components are closely related and should be treated consistently. In an earlier generation of (uncoupled) models, dynamical transport was fixed, and often adjusted separately, possibly in a manner inconsistent with the predicted ozone. When used in a predictive mode, such models may possibly yield incorrect results for future ozone changes.

Because of the physical self-consistency demanded by coupled models, individual components of the model are no longer separately adjustable. Severe constraints are placed by the physical equations of mass, energy, and zonal and meridional momenta. In other words, many formerly adjustable, empirical parameters are now replaced by physical equations of motion, and these are determined either from first principles, or through testable assumptions (such as isentropic versus cross-isentropic mixing by large scale waves, see later discussion).

A zonally averaged (2-D) model with coupled dynamics, radiation and chemistry has been constructed. Our model uses an accurate and efficient radiative transfer module and fairly complete O_x, HO_x, NO_y, Cl_y and hydrocarbon chemistry. Approximately 40 species are treated in 87 photochemical reactions. Both radiative and photochemical codes are described in this paper, the former in a concise format since a detailed documentation is reserved for a separate paper (see Olaguer et al. 1990). The dynamical component of the model has been documented in Yang et al. (1990). The model is formulated in isentropic coordinates

Corresponding author address: Dr. K.-K. Tung, Dept. of Applied Mathematics, FS-20, University of Washington, Seattle, WA 98195.

(Tung 1982, 1984, 1986; Yang et al. 1990) and is nonlinear (nongeostrophic). The present version uses observed temperature as input, and from it both advective and diffusive transports are determined in a self-consistent manner, together with *predicted* ozone and other radiatively active gases. [There is no need to input the observed ozone field in the radiative transfer calculations.] There are *no* tunable transport parameters in the model stratosphere because they are all determined once the zonal mean temperature is specified from observations. It is in this regard that our present coupled 2-D model is unique and is ideally suited to testing our understanding of the physical processes involved in determining the distribution of the chemical species in the present-day atmosphere. The restriction to the diagnostic mode for the present-day atmosphere is the price that one needs to pay: without the observed temperature as input, some eddy quantities become unknown and need to be somehow specified. In the interactive model of Brasseur et al. (1990), an advanced closure scheme for Rossby wave mixing due to Hitchman and Brasseur (1988) is adopted, which nevertheless requires the specification of an empirical "Rayleigh friction" profile, and the resulting Rossby wave mixing coefficient adjusted to be no lower than a floor value of 3×10^9 cm^2 s^{-1} (cf. Yang et al. 1990, where a lower value of 1×10^9 cm^2 s^{-1} was found to be prevalent in the tropical region). Furthermore their model circulation needs to be independently and arbitrarily tuned at the 15 km level to produce a reasonable temperature and tracer mixing ratio slopes. A closure scheme is absent in the interactive model of Schneider et al. (1989) and Schneider and Ko (1990), where both the Rayleigh friction profile and the eddy mixing coefficient are empirically specified. No ad hoc tuning of the circulation at 15 km is done, however, in contrast to the model of Brasseur et al. (1990). Although some tunable parameters still remain in these models, their number is greatly reduced from the previous generation of models (see Harwood and Pyle 1975; Garcia and Solomon 1983; Ko et al. 1984). If in addition the observed temperature is known, the number of empirical parameters can be reduced to zero if all the zonal mean equations of motion are used and if it can be assumed that the dominant process of mixing of tracers and Ertel's potential vorticity occurs predominantly along isentropic surfaces. This is the assumption that we will make in the present work and it will be tested with our model results.

We believe that, because of more physical constraints placed on the model, more physical conclusions can be drawn from the model results. A correct simulation, as compared to the observed distribution, may be viewed as a possible evidence in support of the assumptions about the dominant physical processes incorporated in the formulation. An incorrect simulation may signal a physical deficiency in the model, and, because it cannot be remedied by simply adjusting the transport parameters as was done in the previous generation of models, may suggest new directions in thinking concerning model formulation. For this purpose, we will be particularly interested in looking for *systematic* discrepancies of the model results compared with satellite and other data.

As a further constraint, *many* chemical species will be simultaneously simulated in a coupled fashion including "upward diffusing" and "downward diffusing" species and species with various lifetimes and meridional and vertical gradients. Greater confidence in model formulation can presumably be gained if a simultaneous close fit of all species with observation can be achieved.

2. Dynamics

In a zonally averaged model, the main circulation can be viewed as "driven" by large-scale wave irreversible mixing, in the form of an Eliassen-Palm flux divergence. Because such E-P flux forcing changes from year to year and month to month in a manner not yet predictable by our present understanding of the atmosphere, it needs to be somehow specified or deduced for the year (or month) of interest. (The time period of interest in the present paper is determined by the time period of data collected for comparison.) In the present diagnostic version of our model, the E-P flux divergence is deduced from the observed zonal mean temperature. This has been done using the daily NMC temperature data for the 10-year period from 1979 to 1988, which were kindly provided to us by Drs. David Wu and Eric Nash of NASA (Geller and Wu 1987). The procedure and result were presented in a recent publication (Yang et al. 1990) using the isentropic coordinate formulation of Tung (1986), with recent modification to account for isentropes that intersect the ground. The vertical coordinate used is

$$\frac{z_1}{H} = \frac{\ln(\theta/\theta_o)}{\ln(\theta_c/\theta_o)} \tag{1}$$

where $H = 7$ km, θ is potential temperature, $\theta_c = 350$ K, $\theta_o = 263$ K for $\theta \geq \theta_c$ and $\theta_o = \theta$(surface) for $\theta < \theta_c$.

Let an overbar ($\bar{}$) denote zonal average, ϕ be latitude; $y \equiv a \sin\phi$; V, W be mass flow rates in meridional and vertical directions, respectively; and σ be the air density in the z_1-coordinate, i.e., $\sigma = \rho \partial z / \partial z_1$.

a. Dynamical equations

- Equation of thermodynamics

$$\bar{W} \approx \bar{\sigma}\left[\frac{\bar{Q}}{\bar{\Gamma}} + \min\left(0, \frac{z_1}{H} - 1\right)\left(\frac{\bar{Q}}{\bar{\Gamma}}\right)_s\right] \tag{2}$$

where $\Gamma = T \ln(\theta_c/\theta_o)/H$. This is used to calculate the vertical (diabatic) advective velocity from $\bar{Q}$, the net

diabatic heating rate. The latter is itself calculated using a comprehensive radiative transfer code given the input temperature $\bar{T}$. Subscript s denotes evaluation at the surface. Above one scale height in z_1, $\bar{W}$ is given simply by $\bar{W} \approx \bar{\sigma}\bar{Q}/\bar{\Gamma}$. That is, $\bar{W}$ is the *diabatic* vertical velocity. At the surface, $z_1 = 0$, we have $\bar{W} \equiv 0$, as the two terms in (2) cancel. This can be shown to be exactly true from the definition of $z_1 = 0$.

- Equation for conservation of mass

$$\frac{\partial}{\partial t}\bar{\sigma} + \frac{\partial}{\partial y}\bar{V} + \frac{\partial}{\partial z_1}\bar{W} = 0. \tag{3}$$

This is used to deduce meridional velocity, knowing the vertical velocity and time rate of density change. The latter is calculated from the same temperature time series.

- Equation for zonal momentum

$$\bar{\sigma}\frac{\partial}{\partial t}\bar{L} + \bar{V}\frac{\partial}{\partial y}\bar{L} + \bar{W}\frac{\partial}{\partial z_1}\bar{L} = \Box \cdot F \tag{4}$$

where $L = [u + \Omega a \cos\phi]\cos\phi$ is the absolute zonal angular momentum divided by a, the radius of the earth, Ω is the speed of earth's self-rotation, and $\Box \cdot F$ is the Eliassen-Palm flux pseudodivergence as defined in Tung (1986), which is determined from this zonal momentum budget. In the present isentropic coordinate formulation, there is no need to define a residual circulation as in the case of pressure coordinate formulation. The semi-Lagrangian property of the isentropic coordinates implies that the zonal-mean velocities in this coordinate system are the same as the mean velocities with which the tracers are transported (the so called "transport velocities", WMO 1986) if the waves are adiabatic.

- Equation for meridional momentum

$$f\bar{u} + \frac{\bar{u}^2 \tan\phi}{a} = -\frac{1}{a}\frac{\partial}{\partial\phi}\bar{\Phi} + c_p\bar{T}\left(1 - \frac{z_1}{H}\right)\frac{1}{a}\frac{\partial}{\partial\phi}\ln\bar{\theta}_o. \tag{5}$$

This equation is used to deduce the zonal mean velocity $\bar{u}$ and zonal momentum from the input temperature, as discussed in more detail in Yang et al. (1990). The last term in (5) would be absent if θ is used as the vertical coordinate instead of the hybrid z_1 coordinate.

- Equation for the isentropic flux of Ertel's vorticity $\hat{P} \equiv -\bar{\sigma}^{-1}\partial\bar{L}/\partial y$

$$\frac{\Box \cdot F}{\bar{\sigma}} = -K_{yy}\cos^2\phi\,\frac{\partial}{\partial y}\hat{P}. \tag{6}$$

The last equation is a closure parameterization that assumes that large-scale mixing occurs predominantly along isentropic surfaces. This assumption appears to be valid in the lower and middle stratosphere in some space and time averages, but may break down in the upper stratosphere and mesosphere (see Tung 1987; Yang et al. 1990), where breaking gravity waves may induce significant vertical mixing (Lindzen 1981a; Garcia and Solomon 1985). In contrast to formulations in other coordinate systems, thermal damping of potential vorticity does not play an important role in the conservation equation of Ertel's potential vorticity when the isentropic coordinate system is used (Haynes and McIntyre 1987; Tung 1986; Yang et al. 1990).

The derivation of these equations was given in Yang et al. (1990), and the perfect gas law and hydrostatic equations, not listed, were also used in the derivation. In the earlier generation of (uncoupled) models, the momentum equations were not used, and the isentropic mixing coefficient, K_{yy}, was specified instead of deduced.

b. *Transport equation*

The tracer continuity equation (transport equation), for a species whose mass mixing ratio is denoted by χ_i, is

$$\bar{\sigma}\frac{\partial\bar{\chi}_i}{\partial t} + \bar{V}\frac{\partial\bar{\chi}_i}{\partial y} + \bar{W}\frac{\partial\bar{\chi}_i}{\partial z_1} = \frac{\partial}{\partial y}\bar{\sigma}K_{yy}\cos^2\phi\,\frac{\partial\bar{\chi}_i}{\partial y} + \bar{\sigma}\bar{S}_i, \tag{7}$$

where $\bar{S}_i$ is source or sink for species i and can, in general, depend on other species, i.e.,

$$\bar{S}_i = \bar{S}_i(\bar{\chi}_j), \quad j = 1, 2, \cdots, N.$$

Equation (7) is derived by taking zonal average (along isentropic surfaces) of chemical reaction equation of the form describing the (Lagrangian) rate of change of the concentration (per unit mass) of species i due to the production rate S_i:

$$\frac{d\chi_i}{dt} = S_i, \quad \frac{d}{dt} \equiv \frac{\partial}{\partial t} + \mathbf{v}\cdot\nabla. \tag{8}$$

The approximations and assumptions involved have been described in Tung (1982, 1984, 1987) and references therein.

3. Photochemistry

The chemical package for our 2-D isentropic coordinate model is designed to handle the most important reactions involving the families O_x, HO_x, NO_y, and Cl_y. These families are defined here as follows:

$$O_x = O + O(^1D) + O_3$$

$$HO_x = H + OH + HO_2 + 2H_2O_2$$

$$NO_y = N + NO + NO_2 + NO_3 + HNO_3 + HNO_4 + ClONO_2 + 2N_2O_5$$

$$Cl_y = Cl + ClO + HCl + HOCl + ClONO_2.$$

The distinction between the long-lived families and the short-lived species allows us to economize on computer time since only the families themselves need be advected. The short-lived species concentrations are then determined by assuming that they are in chemical equilibrium with other species in the same family. Moreover, the HO_x family as a whole is sufficiently short-lived that its behavior is adequately treated by assuming an equilibrium between its sources and sinks.

Besides the reactive species themselves, we must also consider the source gases from which they are derived. The major gases comprising air are directly specified in our model. These include H_2 (set at 0.5 ppmv), O_2 (21%), and N_2 (78%). The distributions of the other source gases are determined by transport and photodissociation as well as by interactions with the reactive species. These include methane, nitrous oxide, carbon monoxide, and the chlorofluorocarbons. Water vapor is specified in the present calculation using LIMS data above 100 mb (Russet et al. 1984) and climatologic data below 100 mb (Oort 1983). In a separate version, water vapor is transported in the stratosphere and parameterized in terms of in situ and surface temperature in the troposphere. That version, which has a few empirical parameters in the tropospheric water scheme, is not used for the present paper.

A complete list of reactions included in our photochemical model is given in Table 1. The required reaction rates, quantum yields, and absorption cross sections are taken from JPL (1987), whenever possible. The thermal decomposition rate of N_2O_5 and photodissociation cross sections for H_2O, and $CClF_2CCl_2F$, which are not available from JPL (1987), are instead taken from Baulch et al. (1982). Likewise, cross sections for Rayleigh scattering, ozone absorption and molecular oxygen absorption in the Herzberg continuum are as recommended in WMO (1986). Zenith angle-dependent O_2 and NO cross sections in the Schumann-Runge bands are computed from the parameterization of Allen and Frederick (1982).

Photodissociation in the stratosphere is assumed to result from 1) the direct solar beam depleted by gas absorption and in situ Rayleigh single scattering and 2) diffuse radiation resulting from multiple scattering within a cloudy troposphere. The latter component is calculated by assuming that a Lambert surface exists at the ground with the same effective albedo as the troposphere. The lower-atmosphere effective albedo is computed using the adding method (Lacis and Hansen 1974) and delta-Eddington approximation (Joseph et al. 1976). The specification of cloud parameters used in the calculation is described in the next section.

With the exception of certain diurnal reactions governing the N_2O_5 balance, all chemical processes are assumed to take place in daylight. The photodissociation rates are calculated at two distinct solar hour angles and approximately averaged as described in Cunnold et al. (1975). The daylight averaged concentrations of all constituents, assumed to be in chemical equilibrium, are then derived and the 24-hour average photochemical generation rate of each transported species/family is computed by multiplying the daytime production and loss terms by the fractional length of day. The time-dependent ordinary differential equations for the diurnal species, on the other hand, are solved analytically.

A detailed list of chemical balances determining the concentrations of the individual species is relegated to Appendix A.

4. Radiative transfer

The diabatic heating package consists of three separate modules: an infrared radiation code, a solar radiation code, and a latent heating module. The package makes use of accurate yet efficient radiative transfer methods and incorporates the effects of cloudiness and multiple scattering within the troposphere.

Infrared absorbers accounted for in the diabatic heating code are carbon dioxide, ozone, water vapor, methane and nitrous oxide. The carbon dioxide infrared code utilizes the simplified exchange approximation of Fels and Schwarzkopf (1975), in which the cooling-to-space contribution is calculated from a random model, while the atmospheric layer exchange terms are computed using an empirical broadband emissivity parameterization. The CO_2 emissivity is taken from Ou and Liou (1983) and is based on a polynomial fit to the line-by-line calculations of Fels and Schwarzkopf (1981).

For the cooling-to-space calculation, the wavenumber band from 450 to 900 cm^{-1} is divided into N subintervals of uniform width. Following the suggestion of Crisp et al. (1986), the total Voigt absorptance for each subinterval is computed from the absorptances in the weak, Lorentz and Doppler limits by applying the empirical interpolation formula of Rodgers and Williams (1974) to the entire subband. For simplicity, the Doppler line shape is assumed to be rectangular (Fels 1979). Two distinct random models, RM1 and RM2, are used to simulate the line strength distribution depending on the altitude region. RM1 applies to pressures greater than 1 mb and consists of a Malkmus (1967) model with 90 subintervals. RM2 applies to pressures less than 1 mb and employs a Goody (1952) distribution for strong lines ($S > 10$ cm g^{-1}) and an $S^{-5/4}$ distribution for weak lines ($S < 10$ cm g^{-1}) over the entire 15 micron band (Crisp et al. 1986). Our approach for calculating the Voigt absorptance above the 1 mb level differs from that proposed by Crisp et al. (1986) in that the absorptance in the Lorentz limit is calculated using the same analytical line strength distribution as was used to compute the Doppler absorptance. Both RM1 and RM2 employ the Curtis–Godson approximation (Rodgers and Walshaw 1966) and make use of up-to-date line absorption parameters

TABLE 1. List of photochemical reactions..

J_1	$O_2 + h\nu \rightarrow 2O$	k_{45}	$NO_2 + O_3 \rightarrow NO_3 + O_2$
J_2	$O_3 + h\nu \rightarrow O(^1D) + O_2$	J_{46}	$NO_3 + h\nu \rightarrow NO_2 + O$
J_3	$O_3 + h\nu \rightarrow O + O_2$	J_{47}	$NO_3 + h\nu \rightarrow NO + O_2$
k_4	$O_3 + O \rightarrow 2O_2$	l_{48}	$OH + NO_2 + M \rightarrow HNO_3 + M$
l_5	$O + O_2 + M \rightarrow O_3 + M$	J_{49}	$HNO_3 + h\nu \rightarrow OH + NO_2$
l_6	$O + O + M \rightarrow O_2 + M$	k_{50}	$HNO_3 + OH \rightarrow NO_3 + H_2O$
k_7	$O(^1D) + N_2 \rightarrow O + N_2$	l_{51}	$HO_2 + NO_2 + M \rightarrow HNO_4 + M$
k_8	$O(^1D) + O_2 \rightarrow O + O_2$	k_{52}	$HNO_4 + OH \rightarrow H_2O + NO_2$
J_9	$H_2O + h\nu \rightarrow OH + H$	J_{53}	$HNO_4 + h\nu \rightarrow HO_2 + NO_2$
k_{10}	$H_2O + O(^1D) \rightarrow 2OH$	l_{54}	$NO_3 + NO_2 + M \rightarrow N_2O_5 + M$
k_{11}	$H_2 + O(^1D) \rightarrow H + OH$	J_{55}	$N_2O_5 + h\nu \rightarrow NO_3 + NO_2$
k_{12}	$CH_4 + O(^1D) \rightarrow CH_3 + OH$	j_{56}	$N_2O_5 \rightarrow NO_3 + NO_2$
k_{13}	$CH_4 + OH \rightarrow CH_3 + H_2O$	k_{57}	$Cl + O_3 \rightarrow ClO + O_2$
l_{14}	$CH_3 + O_2 + M \rightarrow CH_3O_2 + M$	k_{58}	$ClO + O \rightarrow Cl + O_2$
k_{15}	$CH_3O_2 + HO_2 \rightarrow CH_3OOH + O_2$	k_{59}	$ClO + NO \rightarrow Cl + NO_2$
k_{16}	$CH_3OOH + OH \rightarrow CH_3O_2 + H_2O$	k_{60}	$Cl + CH_4 \rightarrow CH_3 + HCl$
k_{17}	$CH_3O_2 + NO \rightarrow CH_3O + NO_2$	k_{61}	$Cl + HO_2 \rightarrow O_2 + HCl$
k_{18}	$CH_3O + O_2 \rightarrow CH_2O + HO_2$	k_{62}	$HCl + OH \rightarrow H_2O + Cl$
k_{19}	$CH_2O + OH \rightarrow CHO + H_2O$	k_{63}	$HO_2 + ClO \rightarrow HOCl + O_2$
J_{20}	$CH_2O + h\nu \rightarrow CHO + H$	J_{64}	$HOCl + h\nu \rightarrow OH + Cl$
J_{21}	$CH_2O + h\nu \rightarrow CO + H_2$	k_{65}	$HOCl + OH \rightarrow H_2O + ClO$
k_{22}	$CHO + O_2 \rightarrow CO + HO_2$	l_{66}	$ClO + NO_2 + M \rightarrow ClONO_2 + M$
k_{23}	$CO + OH \rightarrow H + CO_2$	J_{67}	$ClONO_2 + h\nu \rightarrow Cl + NO_3$
k_{24}	$OH + HO_2 \rightarrow H_2O + O_2$	k_{68}	$ClONO_2 + O \rightarrow ClO + NO_3$
k_{25}	$H + HO_2 \rightarrow$ products	l_{69}	$ClO + ClO + M \rightarrow Cl_2O_2 + M$
k_{26}	$O_3 + OH \rightarrow HO_2 + O_2$	J_{70}	$Cl_2O_2 + h\nu \rightarrow ClOO + Cl$
k_{27}	$O + OH \rightarrow H + O_2$	k_{71}	$ClOO + M \rightarrow Cl + O_2 + M$
k_{28}	$H + O_3 \rightarrow OH + O_2$	J_{72}	$CCl_4 + h\nu \rightarrow 4Cl +$ products
l_{29}	$H + O_2 + M \rightarrow HO_2 + M$	J_{73}	$CFCl_3 + h\nu \rightarrow 3Cl +$ products
k_{30}	$HO_2 + O \rightarrow OH + O_2$	J_{74}	$CF_2Cl_2 + h\nu \rightarrow 2Cl +$ products
k_{31}	$HO_2 + O_3 \rightarrow OH + 2O_2$	J_{75}	$CH_3CCl_3 + h\nu \rightarrow 3Cl +$ products
k_{32}	$2HO_2 \rightarrow H_2O_2 + O_2$	k_{76}	$CH_3CCl_3 + OH \rightarrow 3Cl +$ products
k_{33}	$H_2O_2 + OH \rightarrow H_2O + HO_2$	J_{77}	$CH_3Cl + h\nu \rightarrow Cl +$ products
J_{34}	$H_2O_2 + h\nu \rightarrow 2OH$	k_{78}	$CH_3Cl + OH \rightarrow Cl +$ products
k_{35}	$N_2O + O(^1D) \rightarrow 2NO$	J_{79}	$CClF_2CCl_2F + h\nu \rightarrow 3Cl +$ products
k_{36}	$N_2O + O(^1D) \rightarrow N_2 + O_2$	J_{80}	$CHClF_2 + h\nu \rightarrow Cl +$ products
J_{37}	$N_2O + h\nu \rightarrow N_2 + O(^1D)$	k_{81}	$CHClF_2 + OH \rightarrow Cl +$ products
k_{38}	$N + NO \rightarrow N_2 + O$	k_{82}	$F + O_3 \rightarrow FO + O_2$
J_{39}	$NO + h\nu \rightarrow N + O$	k_{83}	$FO + O \rightarrow F + O_2$
k_{40}	$N + O_2 \rightarrow NO + O$	k_{84}	$FO + NO \rightarrow F + NO_2$
k_{41}	$NO + HO_2 \rightarrow NO_2 + OH$	k_{85}	$F + CH_4 \rightarrow HF + CH_3$
J_{42}	$NO_2 + h\nu \rightarrow NO + O$	k_{86}	$F + H_2 \rightarrow HF + H$
k_{43}	$NO + O_3 \rightarrow NO_2 + O_2$	k_{87}	$F + H_2O \rightarrow HF + OH.$
k_{44}	$NO_2 + O \rightarrow NO + O_2$		

derived from the HITRAN database tape (Rothman et al. 1987).

The ozone infrared algorithm is a modified version of the parameterization of Rosenfield (1990), who employed separate Goody (1952) random models for the band center (1020 to 1055 cm^{-1}) and wings (980 to 1020 cm^{-1} and 1055 to 1100 cm^{-1}) of the ozone 9.6 micron band. We use the strict Curtis–Godson approximation to treat vertical inhomogeneity, whereas Rosenfield (1990) used a somewhat different absorption path scaling method.

The water vapor infrared scheme employs the nonisothermal emissivity formulation of Ramanathan and Downey (1986) for the pure rotation and vibration–rotation bands. For the two continuum bands, however, we use the simpler isothermal emissivity scheme of Ramanathan (1976), modified to include the temperature dependence of the continuum absorption coefficient (Roberts et al. 1976). Line overlap between water vapor and carbon dioxide is accounted for by multiplying the CO_2 emissivity by the transmission of water vapor at 15 microns. The latter quantity is computed from a single-interval Goody random model as in Rodgers (1967). Line overlap between water vapor and ozone in the 9.6 micron band is likewise accounted for by multiplying the ozone absorptance by the water vapor transmission function of Roberts et al. (1976) evaluated at the band center.

The infrared code also accounts for absorption by methane near 1306 cm^{-1} and by nitrous oxide near 1285 cm^{-1}. The band models for these absorbers are from Donner and Ramanathan (1980).

Heating of the atmosphere due to absorption of solar radiation by ozone, molecular oxygen and nitrogen dioxide is treated by the same basic method used to compute the model photodissociation rates, i.e., heating

is the result of absorption of the direct solar beam and of visible diffuse radiation arising from multiple scattering in the troposphere. The wavelength intervals and photon fluxes used to compute the ultraviolet and visible absorption are from WMO (1986) (we employ the coarser of the two recommended grids for wavelengths beyond 400 nm). The ground albedo is a function of latitude only and is taken from Sellers (1965).

The model treatment of near-infrared absorption by water vapor in a cloudy sky, like that of visible absorption by ozone in the lower atmosphere, is based on the adding method and delta-Eddington approximation. The integration over wavelength, however, is replaced by the k-distribution method as in Lacis and Hansen (1974). The required probability distribution of water vapor absorption coefficients was taken from Somerville et al. (1974). Above the highest cloud top, we assume that in situ scattering is unimportant and treat water vapor absorption using Lacis and Hansen's (1974) clear-sky approach. The ground albedo, however, is replaced by the effective tropospheric albedo as computed in the cloudy-sky case. A similar treatment is employed for near infrared absorption by carbon dioxide above the troposphere, where we have used the empirical expression of Sasamori et al. (1972) for the CO_2 absorptivity. Absorption of solar radiation by carbon dioxide below the tropopause is ignored, since this is insignificant compared to other diabatic processes.

Cloud parameters required for the radiative code are the cloud top heights, cloud cover, the pressure difference across the clouds, cloud emissivities and cloud visible optical depths. The first three of these are specified according to the climatological data of Newell et al. (1974). Cloud emissivities are assumed to be unity, except for high clouds, which are assigned an emissivity of 0.3. Cloud optical depths, on the other hand, are 2, 8, and 16 for high, middle and low clouds, respectively. The infrared heating is computed assuming that the clouds are randomly overlapped. For the multiple scattering computations, the reflection and transmission functions of an atmospheric layer are averaged over clear and cloudy areas.

To complete the specification of the diabatic heating in the troposphere, we include a constraint on latent heating based on the requirement that the horizontally averaged net diabatic heating be zero. The vertically averaged latent heating is constrained by the zonally averaged precipitation rate, which is assumed to vary sinusoidally in an annual wave. Precipitation rates are estimated from rainfall data tabulated by Schutz and Gates (1972a,b) for winter/summer.

The latent heating parameterization is applied to pressure levels below a dimensionless scale height Z_T satisfying:

$$Z_T = \frac{Lq_s}{gH[1 - \langle \gamma_w/\gamma_d \rangle]}$$

where L is the latent heat of vaporization, q_s is specific humidity at the surface, H is atmospheric scale height and $\langle \gamma_w/\gamma_d \rangle$ is the tropospheric average ratio of moist and dry adiabatic lapse rate. This last equation is equivalent near the tropics to the condition of neutral buoyancy for a cloud, that is the level at which a cloud's moist static energy is equal to its moist enthalpy at the ground (Lindzen 1981b). If $\Pi(\phi)$ represents the precipitation rate in mm day^{-1} as a function of latitude ϕ, then the latent heating distribution below Z_T is given by

$$Q_{lh}(\phi, Z) = r(\phi, Z)\bar{Q}_r/\bar{r}(\phi, Z)$$

$$r(\phi, Z) = 0.25\Pi(\phi) + \int_{\exp(-Z)}^{\exp(-Z_T)} Q_{lh}(\phi, Z)dP$$

where $\langle Q_r \rangle$ is the horizontally averaged radiative cooling in K day^{-1}.

The radiative code produces horizontally averaged net heating rates which are very close to zero at most levels above the tropopause, particularly at the dynamically important altitudes. Below the tropopause, it is enforced to be identically zero.

5. Numerics and boundary conditions

The transport equations are solved using time splitting technique. The advection parts of the equations are solved using Prather's scheme (Prather 1986). Shia et al. (1990) have performed a series of experiments and found Prather's scheme to be accurate and suitable for applications to atmospheric transport models. The diffusion terms are discretized such that the area weighted total mass is conserved, taking into account the effect of varying mesh sizes on a spherical earth. The time changes due to chemical source terms are calculated using the backward Euler method to ensure stability. Time step of integration used is 6 hours. The domain of integration is from southern pole to northern pole horizontally, and from surface (1000 mb) to eight scale heights ($z_1/H = 8$) vertically. (The domain is dictated by the availability of NMC temperature data.) Horizontal resolution is 10 degrees in latitude and vertical resolution (evenly spaced in z_1) is about $\frac{7}{3}$ kilometers in stratosphere and approximately 2 kilometers in the troposphere ($\theta < 350$ K). Doubled resolution runs have also been performed to test sensitivity. The sensitivity to vertical resolution occurs mainly in radiative transfer calculations and in the version with transported HNO_3. By performing 1 and 0.5 km calculations for fixed latitudes, we determine that 1 km resolution is sufficient. The differences between 2 and 1 km resolutions are isolated and largely remedied. Mass flow rate is zero at the two poles and at the top of domain (solid lid condition). Vertical velocity is zero at $z_1 = 0$ by definition with our choice of vertical

coordinates. The transported species/families include O_x, NO_y, N_2O, CH_4, CO, Cl_y, CFCs and HF.

The following lower boundary conditions are used: $O_x = 20$ ppbv, $NO_y = (1 - 0.7\cos\phi)$ ppbv, $N_2O = 315$ ppbv, $CH_4 = 1.6$ ppmv, CO = 0.6 ppmv, $Cl_y = 0.0$, HF = 0.0, F10 = 80 pptv, F11 = 173 pptv, F12 = 297 pptv, $CH_3CCl_3 = 105$ pptv, $CH_3Cl = 600$ pptv, F113 = 15.3 pptv, and F22 = 54 pptv.

The boundary values of the source gases can be specified to change according to certain scenarios. For our present purpose, however, they are fixed at the present-day (1980) observed values.

6. Simulation of the present-day composition

The state of the atmosphere changes from year to year and the model should somehow know which year it is simulating. For the present work, the year (and season) is chosen based on when an observation that we use to compare our results with was taken. Then the observed temperature for that particular period is used as input to our 2-D model. As described in Tung (1987), this input then fixes the dynamical parameters for that period. They are used to transport the chemical trace gases, the simulated results for which are then compared with observations.

The zonal mean temperature $\bar{T}$ that we use as input for the diagnostic model has been processed from a three dimensional, daily NMC dataset, which is made available to us by E. Nash and D. Wu of NASA for the period from December 1978 to November 1988. The zonal average is taken on surfaces of constant z_1 as described in Yang et al. (1990). The input data is updated every 5 days, at which time a new diabatic heating, $\bar{Q}$, is calculated.

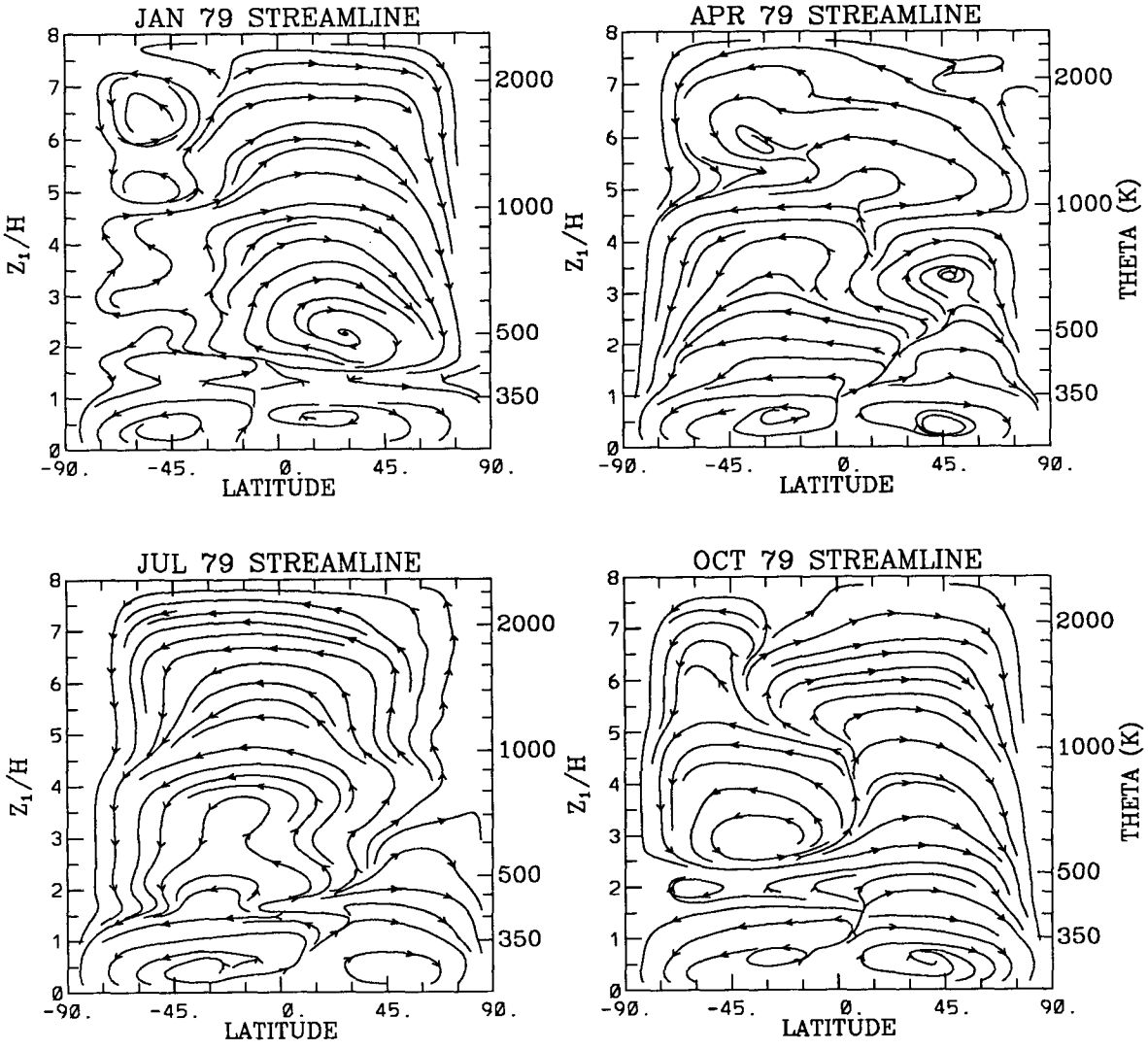

FIG. 1. Streamlines for velocity field ($\bar{V}$, $\bar{W}$) for 1979.

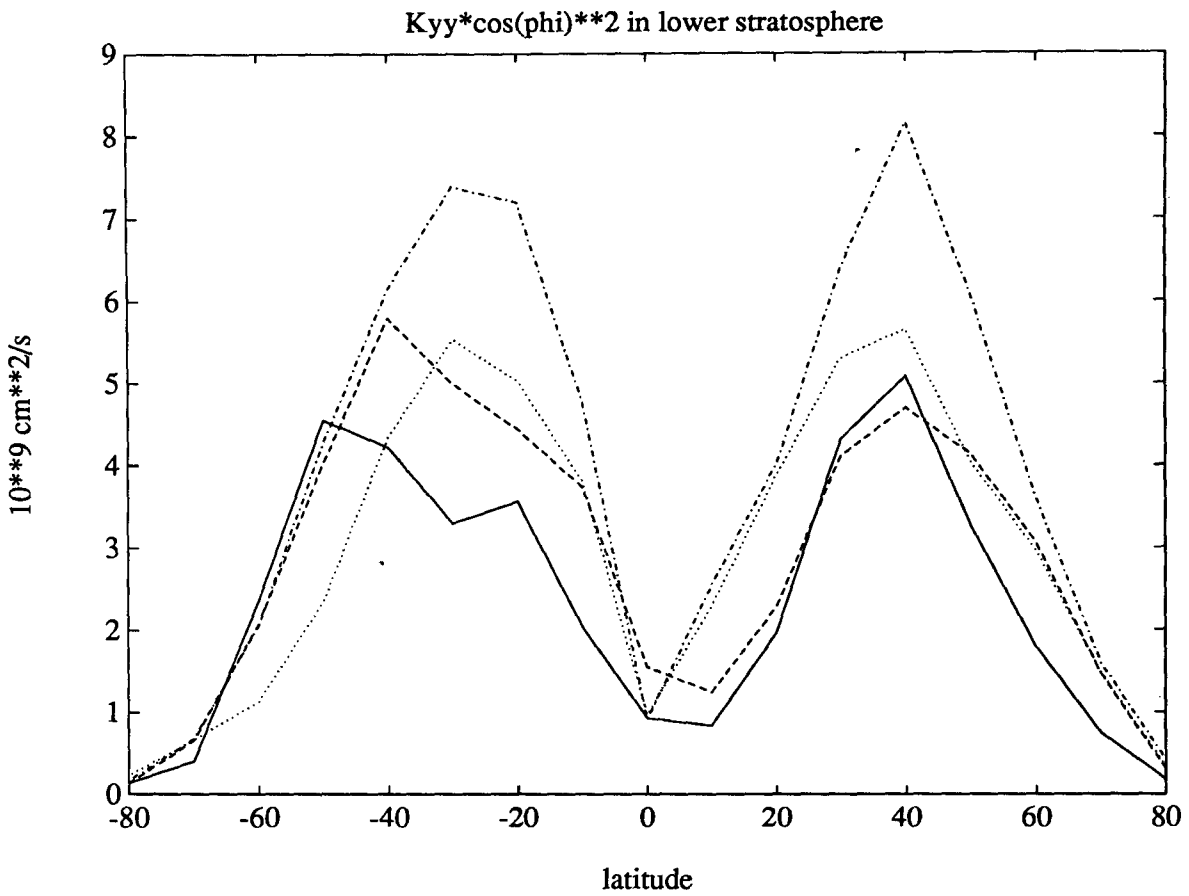

FIG. 2. Values of $K_{yy} \cos^2\phi$ averaged from 13 to 25 km for 1979 (Solid line for January dashed line for April, dotted line for July, and dash-dotted line for October).

Since 1979 is our first complete year of temperature input, all of the runs start from January 1, 1979. For most species, detailed initial conditions are not available. These are instead generated within the model by running the model through many annual cycles using 1979 temperature data until annual periodicity is achieved. Several (about seven) model years are required before such periodicity is reached if one starts from the state of photochemical equilibrium. In some subsequent runs, the results of an earlier run are used to "spin up" the model to save computation time. In such cases, the first annual cycle is disregarded before any results are obtained. In all cases, annually quasi-periodic conditions are reached with 1979 transports before new inputs are given.

Transport parameters

The streamlines for the advecting mean velocity field ($\bar{V}$, $\bar{W}$) is shown in Fig. 1 for the months of January, April, July and October of 1979. The K_{yy} field[1] in the lower stratosphere (average of layer from 13 to 25 km) is shown in Fig. 2 for the same four months. In general, the K_{yy} field is small (on the order of 1×10^9 cm^2 s^{-1}) over the equatorial region and over both poles but reaches a maximum value of 5 to 6×10^9 cm^2 s^{-1} near the latitude of 40 degrees in both hemispheres (near the equatorward flank of the jet maxima).

7. Ozone

Ozone is produced through the photodissociation of molecular oxygen, mainly in the stratosphere ($\sim$35 km). It is destroyed directly by photodissociation and reactions with atomic oxygen, indirectly through catalytic cycles involving the families HO_x, NO_y, and Cl_y. Transport plays an important role in bringing ozone from the photochemical source region (tropical upper stratosphere) into higher latitudes and lower altitudes, where chemical processes are no longer dominant in determining local ozone mixing ratios. Because of this interplay between photochemistry and dynamical transport, the total column density of zonal mean ozone exhibits interesting seasonal and latitudinal be-

[1] Note that because of our definition of $y = a \sin\phi$, the quantity $K_{yy} \cos^2\phi$ is equivalent to the usual K_{yy} when y is defined to be $a\phi$.

havior. The most recent analysis of the SBUV satellite measurements of atmospheric ozone can be found in Jackman et al. (1989). The average of these measurements for the three-year period 1979–81 is shown in Fig. 3. A similar time average of results from a 3-year run of our 2-D model using daily NMC temperatures for the period 1979–1981 is shown in Fig. 4. The observed SBUV data were further divided by Jackman et al. (1989) into column densities for three layers: 1000–100 mb, 100–10 mb and 10–1 mb. These are shown in Fig. 5. The simulated layer averages are shown in Fig. 6. The model ozone mixing ratio is shown in Fig. 7.

All major features of the observed seasonal and latitudinal variations are reproduced by the model simulation. For the total column ozone (shown in Figs. 3 and 4 for the observed and simulated, respectively), the agreement between the model simulation and observation is very good. The spring maximum (SBUV: 460 DU; model: 460 DU) and fall minimum (SBUV: 300 DU; model: 320 DU) in the Northern Hemisphere have been correctly simulated, both in timing and duration to within the uncertainty of data. In our earlier version using the Newtonian cooling approximation (Tung and Yang 1988), the high latitude spring maximum lasted too long and the fall minimum was less prominent. The problem was due to a lack of time resolution in the radiative equilibrium temperature field; only an annual harmonic was used. Therefore, the radiative field during periods of rapid change in the solar radiation at high latitudes was not adequately simulated. The same problem exists in other models using Dopplick's (1972, 1979) and Murgatroyd and Singleton's (1961) solstice heating rates fitted to an annual harmonic. In the present model, radiative heating rates are calculated every five days.

In the Southern Hemisphere the polar spring minimum (SBUV: <280; model: 260 DU) and subpolar maximum (SBUV: 380 DU; model 380 DU) are also reproduced. The rapid final warming in late spring (November) when the subpolar maximum is mixed in with the polar minimum is correctly reproduced, both in timing, duration and in magnitude. During this period of time, warmer air with high ozone concentrations from the subpolar latitudes is mixed rapidly into the polar vortex, resulting in a strong sinking motion over the polar region. Without a time-varying K_{yy}, this rapid event cannot be simulated in a *coupled* model. In the model of Schneider and Ko (1990), a slowly varying K_{yy} (winter–summer–equinox) field was specified, the warming consequently lasted for more than 3 months into the summer. Also, when no north–south asymmetry is present in their K_{yy} field, the Southern Hemisphere column ozone is the same as its northern counterpart, shifted by six months.

The equatorial minimum is present in the model result with the correct seasonal variation. The SBUV data show tropical ozone values of about 260 Dobson units, while the model simulation gives ozone values of about 20 Dobson units lower due largely to 40-km ozone deficit. Note, however, that TOMS ozone is about 20 Dobson units lower than SBUV in the tropics (Bowman and Krueger 1985) and thus closer to our model ozone.

Although the total column density of ozone is affected by both chemistry and dynamics, the seasonal and latitudinal variations appear to be controlled almost entirely by dynamical transport. A discussion of mechanistic explanations of the major features in the latitude–season map of column ozone can be found in Tung and Yang (1988) and in Ko et al. (1989). Additional comments will be made later in this section.

It is noteworthy to mention here that we have performed a control run where all seasonal and latitudinal variations in the photochemical sources and sinks of ozone are artificially suppressed, and the same qualitative features seen in Fig. 4 still remain. In Fig. 8, we show the column density of a fictitious tracer Z (Jackman et al. 1989) transported with our circulation and K_{yy} for 1980. The tracer has *no* latitudinally and seasonally varying chemical sources. It is prescribed to be uniformly 8 ppmv above 10 mb for all latitudes and seasons and 0.01 ppmv near the ground. There are no chemical sources or sinks below 10 mb. It is amazing how similar this Dütch map is compared with that for ozone.

An examination of separate layer averages serves to reiterate the point just made. All the latitudinal and seasonal features in the total column ozone in Figs. 3 and 4 are present in the middle layer (100–10 mb) in Fig. 5b for SBUV data and Fig. 6b for the model simulation. In fact, one can say, for both the observed and simulated ozone, the middle layer is responsible for the seasonal and latitudinal variations in the total column. Ozone in this layer in the lower stratosphere can be regarded as a long-lived tracer and is known to be affected predominantly by transport. Again, the simulation compares favorably with data both qualitatively and quantitatively. Both show a winter and early spring maximum (SBUV: 260 DU; model 280 DU) and a fall minimum (SBUV: 180 DU; model 200 DU) in Northern Hemisphere. Both show a spring polar minimum ($\sim$160 DU) and a subpolar maximum (SBUV: 240 DU; model 260 DU) in Southern Hemisphere.

Fairly favorable comparison also holds for overall patterns in the lower layer (1000–100 mb) as can be seen from Figs. 5a and 6a, with 40 DU in the $\pm 30°$ region, 80 DU in Southern subpolar region and 120 DU near 60°N. The Northern fall minimum in the model is however not as pronounced as in the SBUV data, contributing to the 20 DU overprediction of the fall minimum in the total column. [Note that the observed data for this layer are comprised primarily of climatological measurements.] We would like to point out that the diabatic circulation in the troposphere has a high level of uncertainty, due, among other things,

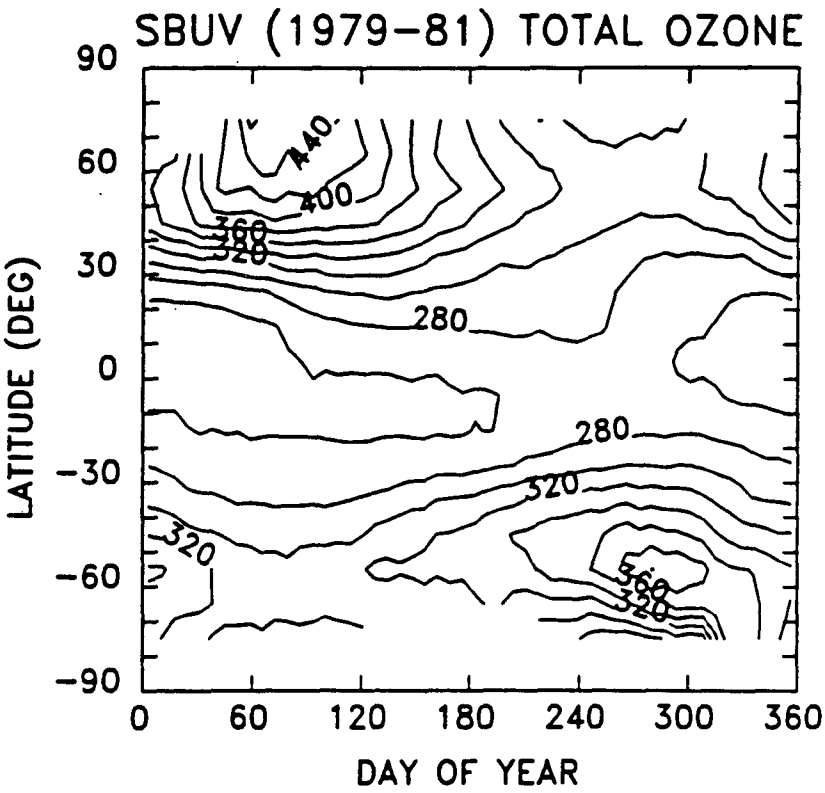

FIG. 3. Three-year (1979–81) average SBUV total ozone (in Dobson units) (taken from Jackman et al. 1989).

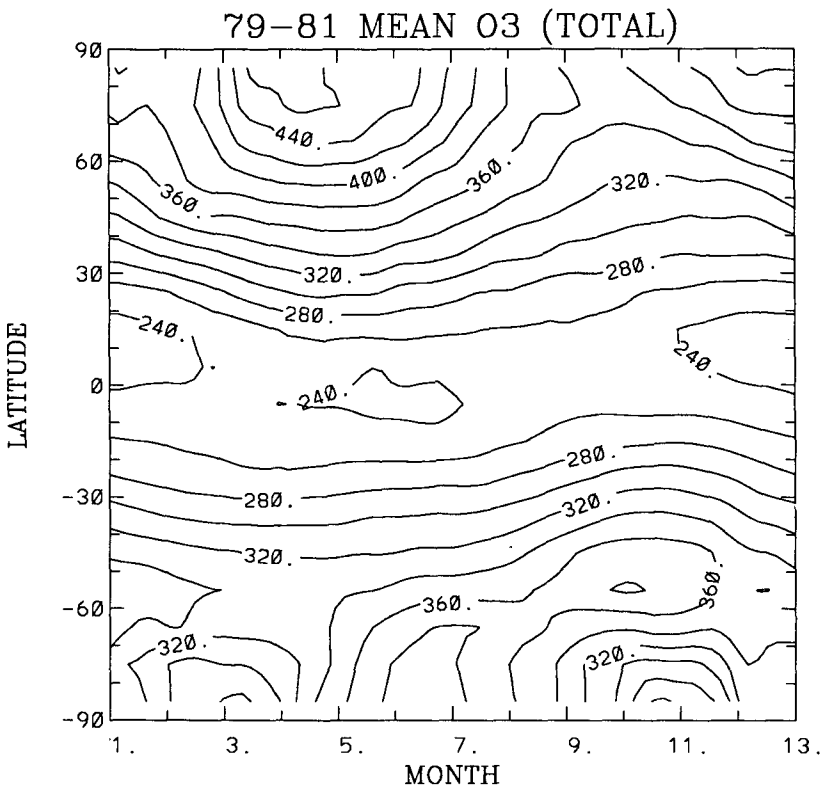

FIG. 4. Three-year (1979–81) average model simulated total ozone (in Dobson units).

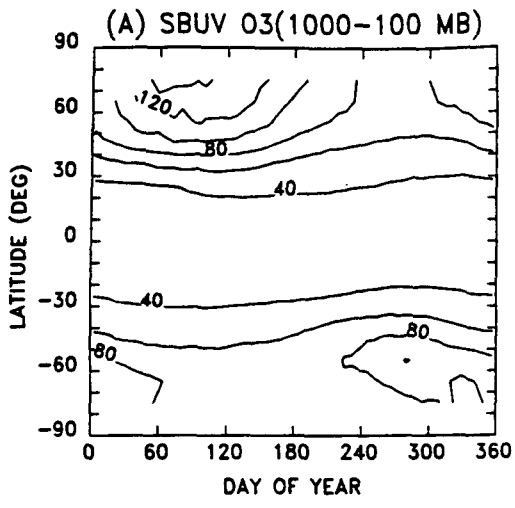

FIG. 5. SBUV total ozone (in Dobson units) in three layers: (a) 1000–100 mb; (b) 100–10 mb; (c) 10–1 mb (taken from Jackman et al. 1989).

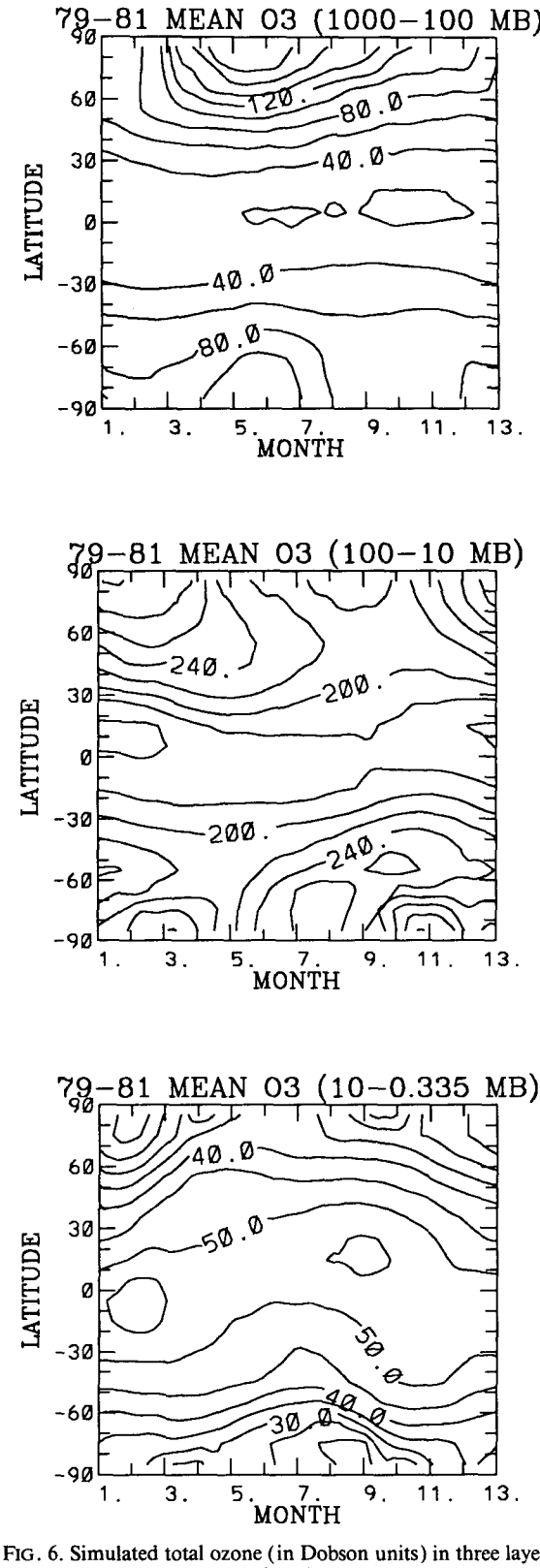

FIG. 6. Simulated total ozone (in Dobson units) in three layers: (a) 1000–100 mb; (b) 100–10 mb; (c) 10–0.335 mb.

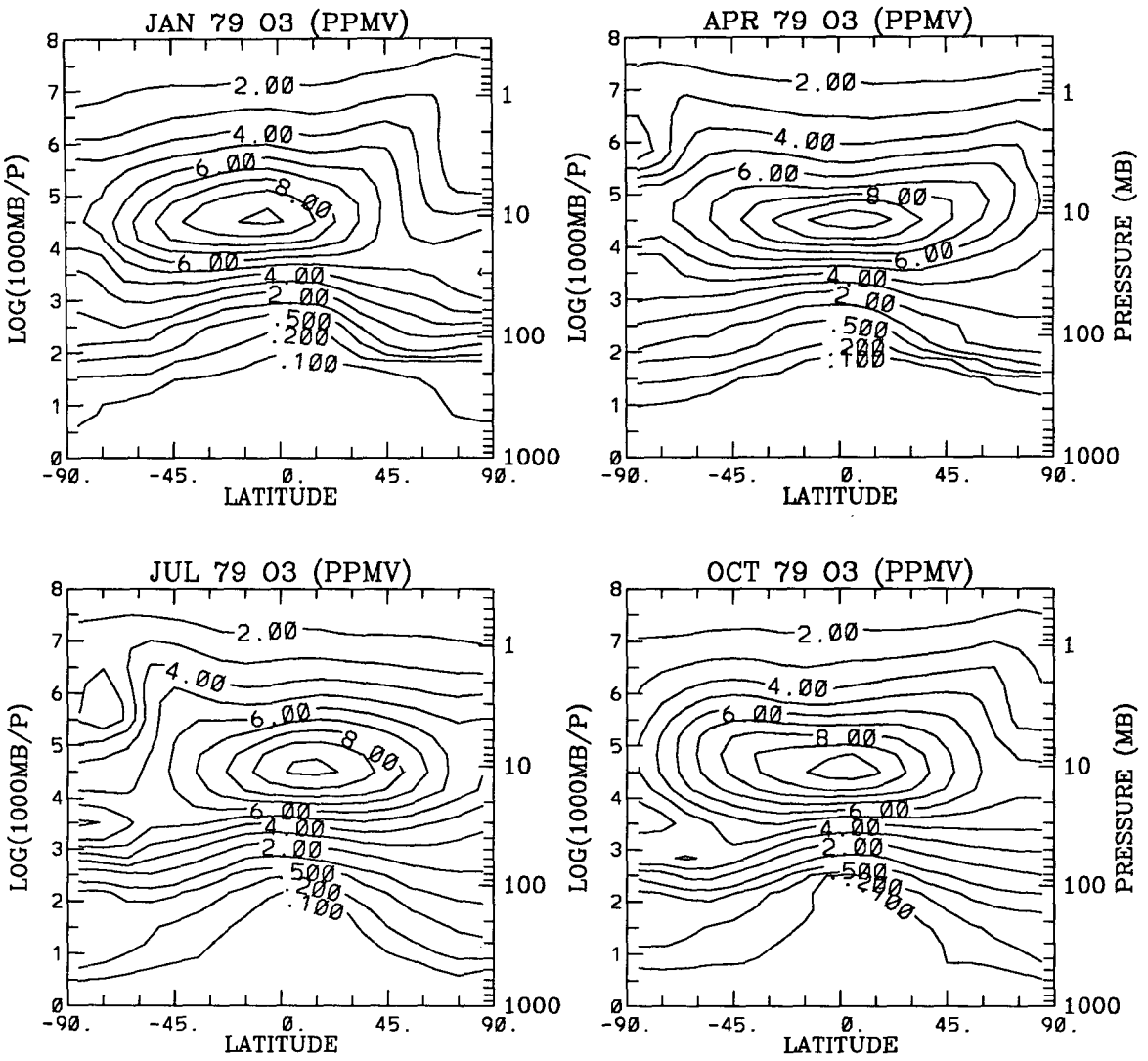

FIG. 7. Simulated ozone mixing ratio for 1979.

to the uncertainty in latent heating, and the in situ radiative effects of clouds. Also, no vertical mixing is adopted in the present version.

In the upper layer, ozone is dominated by photochemical processes. Figures 5c and 6c show that our model result is about 10 Dobson units (15%) too low compared with SBUV data, but all the seasonal and latitudinal features are otherwise correctly simulated. A deficit of model ozone near 40 km compared with SBUV or LIMS observations is common among both 1-D and 2-D models (see WMO (1986) and Jackman et al. (1986) for a review), and was thought to be probably related to a missing source or an overestimate of chemical sinks of ozone in the upper stratosphere. Allen et al. (1990) recently proposed that it is the satellite data that are too high.

Returning to the total column amount, we mention here that although the latitudinal and seasonal variations are known to be caused by dynamical transports, it is not clear which feature is caused by which kind of transport (advection vs diffusion). It is apparent that the qualitative features are caused by the variations in the diabatic circulation, but quantitatively the maxima and minima can be affected greatly by diffusive transport. In an earlier generation of 2-D models which use a constant diffusion coefficient, a common problem has been having ozone spring maximum of over 600 Dobson units (see Ko et al. 1985b). Some groups have subsequently tuned their diabatic circulation to reduce this maximum value to within the observed limits, while it is perhaps the K_{yy} latitudinal and seasonal distributions that should have been changed. We have repeated our calculation, using a constant $K_{yy}\cos^2\phi$ of 3×10^9 cm^2 s^{-1}, but with the same diabatic circulation, and found all major features in Fig. 4 remain intact, except that the winter–spring maximum in the North-

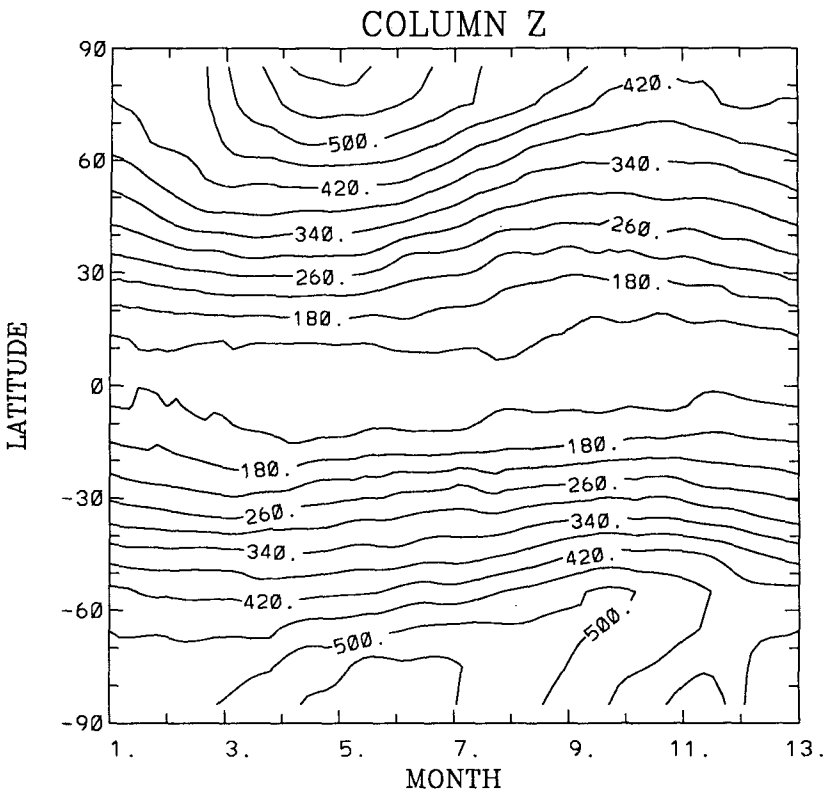

FIG. 8. Total column of Z in Dobson units (see text).

ern Hemisphere now becomes much more intense, reaching values of over 600 Dobson units and lasting longer than the observed.

Year-to-year variations

Individual years are simulated using NMC temperature specific to each of the years. The column ozone for 1979–1982 from the model is shown in Fig. 9. The year-to-year variations can be quite large (more than 50 DU) at high latitude, while the variation in the tropics are moderate. The Northern spring maximum varies in both magnitude and in timing. In the Southern Hemisphere, deeping of the "ozone hole" in the spring ozone minimum from its higher 1979 value is apparent. Compared to the 10-year climatology (although only results of four years are shown here, we have performed calculation for the 10-year period of 1979–88), the year 1979 is abnormally warm during winter and so the spring ozone minimum (in the "ozone hole") is abnormally high (see also Tung and Yang 1988). The year 1981 is more quiescent during winter and spring, the winter ozone values are constant until in early August, then dropping lower until middle October when a minimum is obtained. Note also that the model winter Southern polar maximum, which occurred during June and July in 1979 and 1980 disappeared in later years, an indication that the polar vortex is more leaky in earlier years than in later years.

No heterogeneous ozone reactions are incorporated in the present calculation. Consistent with our earlier results (see Tung and Yang 1988; and Yang et al. 1989), it appears that the year-to-year variations of Antarctic ozone can be reasonably simulated for the early part of the decade (1979–88) without heterogeneous chemistry but with prescribed temperature variation. In later years, however, the model ozone hole values are increasingly and systematically higher than the observations.

8. Odd nitrogen

NO_y

The source of NO_y is the gas N_2O, which reacts with $O(^1D)$ to produce two molecules of NO for every molecule of N_2O. NO_y is destroyed when N and NO combines to form N_2 and O. Ko et al. (1986) and Jackman et al. (1987) pointed out that there was a serious *common* model deficiency in NO_y in the equatorial lower stratosphere, by up to an order of magnitude, when compared to LIMS observations. Figure 10, taken from Ko et al. (1986), shows this typical model deficiency in the equatorial lower stratosphere.

It was speculated that perhaps a physical source of odd nitrogen was missing in all 2-D models. Ko et al. (1986) suggested that lightning might be a possible missing source and, through a sensitivity study, chose

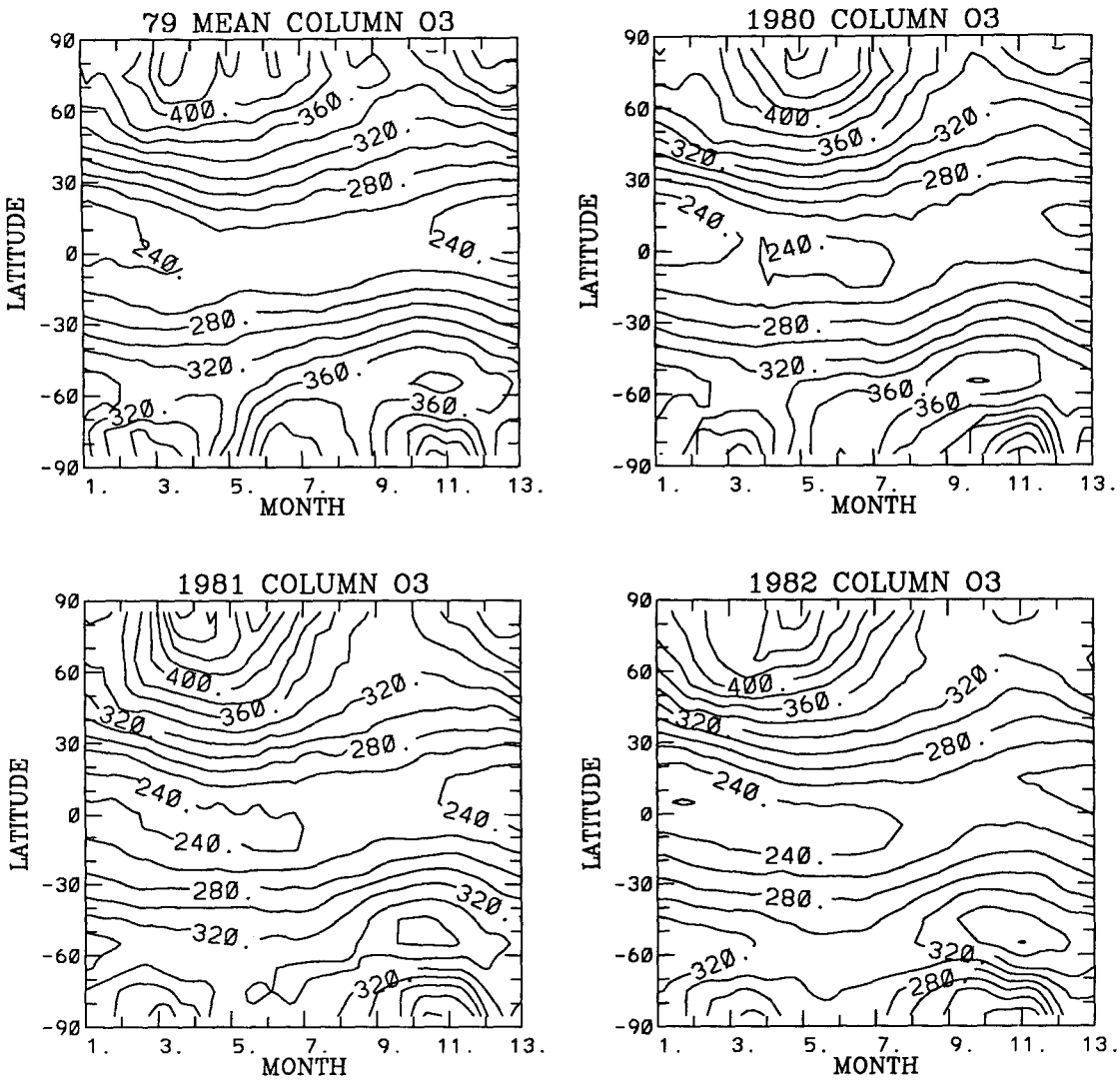

FIG. 9. Model simulated total ozone in Dobson units for 1979–82.

an empirical value for the source strength that brought the AER model odd nitrogen to the observed range. Many groups subsequently adopted a lightning source with the magnitude chosen by Ko et al. (1986). It turns out, however, that different models require different amounts of "missing source" in order to fit the data. For example, Jackman et al. (1989) found that even with the (H2) source of Ko et al., their modeled NO_y is still much lower than observed in the lower stratosphere. It appears (see later discussion) that the strength of equatorial upwelling can have an important impact on the NO_y values in the lower stratosphere and that most of the models have too strong an equatorial upwelling.

While it is probably true that lightning can provide an important source of odd nitrogen, the magnitude and height of deposition of such a source are at present very uncertain. Since the justification for its inclusion in models at this stage is based on a perceived common model deficiency, it is perhaps useful to perform a revised analysis of this problem using our latest model without a lightning source.

Even without such a source, our model does not show a significant deficiency in odd nitrogen. In Fig. 11, we show LIMS measurement of nighttime NO_2 + HNO_3 + 2(model N_2O_5) taken from WMO (1986), which should constitute the bulk of total odd nitrogen. Our model total odd nitrogen is shown in Fig. 12, which compares favorably with LIMS. In particular, no significant deficiency is noted in the equatorial lower stratosphere.

To address the issue of reliability of LIMS infrared NO_y, a comparison of LIMS (infrared) and ATMOS (direct) measurements at 30°N was presented by Russell et al. (1988) and is reproduced here in Fig. 13, along with our model vertical profile at the same lati-

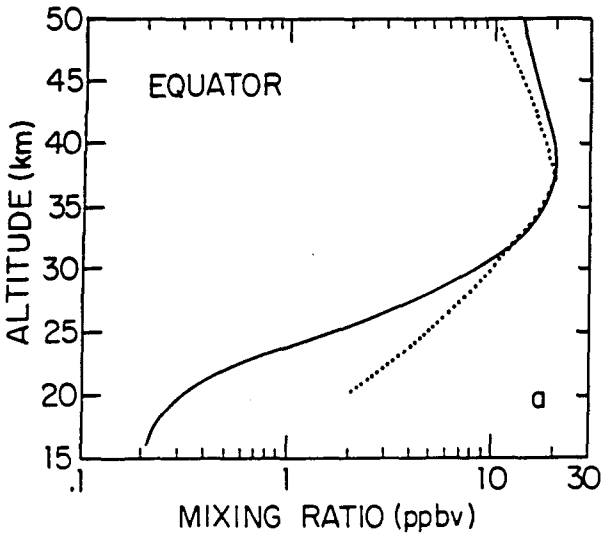

FIG. 10. Comparison of the calculated NO_y profile of Ko et al. (1986) (solid line) with the observed nighttime concentration of NO_2 and HNO_3 (taken from Ko et al. 1986).

tude. [ATMOS data (Russell et al. 1988) is for 1 May 1985. LIMS is for 1 May 1979.] Above 40 km, ATMOS is higher than LIMS (and our model result). At 36 km, near the NO_y peak, LIMS (and our model result) is higher than ATMOS. LIMS and ATMOS agree in the lower stratosphere, while our model is slightly higher at 30°N.

Unfortunately, ATMOS data are not available over the equator, where most of the deficit occurs in previous model results. A detailed comparison of the latitudinal behavior of several 2-D model results with LIMS inferred NO_y at 3, 16 and 30 mb has been given in WMO (1986). In Fig. 14, that comparison at 30 mb is reproduced here with our present model result for January 1979 (the year of LIMS observations) superimposed. Overall, our present result appears to be the most consistent with data. Over the tropical latitudes, Pyle's model (Harwood and Pyle 1975) comes closest to ours and to LIMS. However, this is due largely to their use of large K_{yy} and K_{zz} diffusion coefficients, and thus the agreement over the tropics comes at the expense of a latitudinal and vertical gradient which are much too small (especially in the vertical direction) when compared to LIMS. Our total odd nitrogen content is about 2 to 3 times larger than those of AER (Ko et al. 1985a) and GS (Garcia and Solomon 1983) in low to middle latitudes.

The fact that NO_y behaves like a quasi-conservative tracer in the whole stratosphere and so is sensitive to the details of transport parameterization may explain the differences between the models mentioned above. It appears that most other models used a diabatic circulation whose upwelling branch over the equatorial lower stratosphere is stronger than ours (see Shia et al. 1989). This circulation brings up too much low NO_y air from the lower stratosphere and may account for the NO_y deficit in the lower stratosphere in most models. This "dynamical loss" by a strong upwelling is counteracted somewhat by an enhanced photochemical production of NO_y due to an increase in N_2O also brought up by the same circulation. However, because of the long photochemical time scales for NO_y in the stratosphere, the counteracting photochemical effect is not significant.

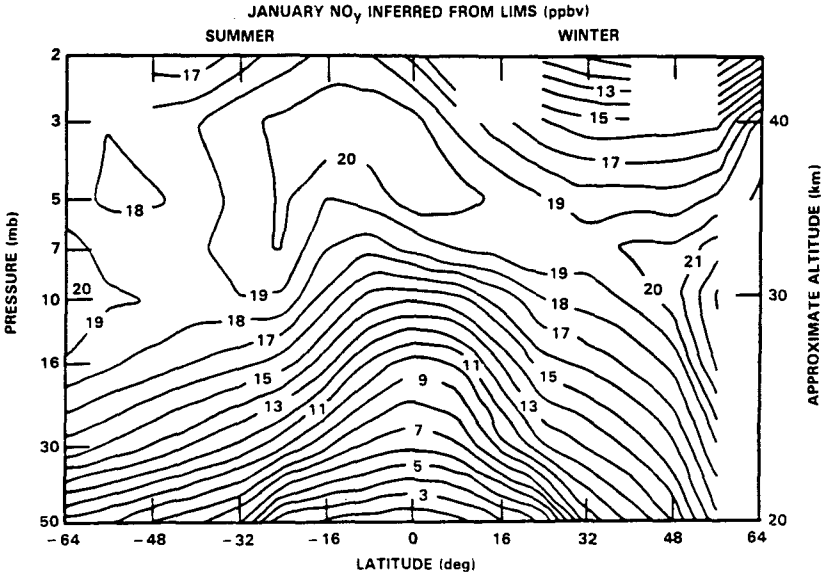

FIG. 11. Distribution of total odd nitrogen inferred from LIMS measurement of nighttime NO_2 and HNO_3 for January 1979 (taken from WMO 1986).

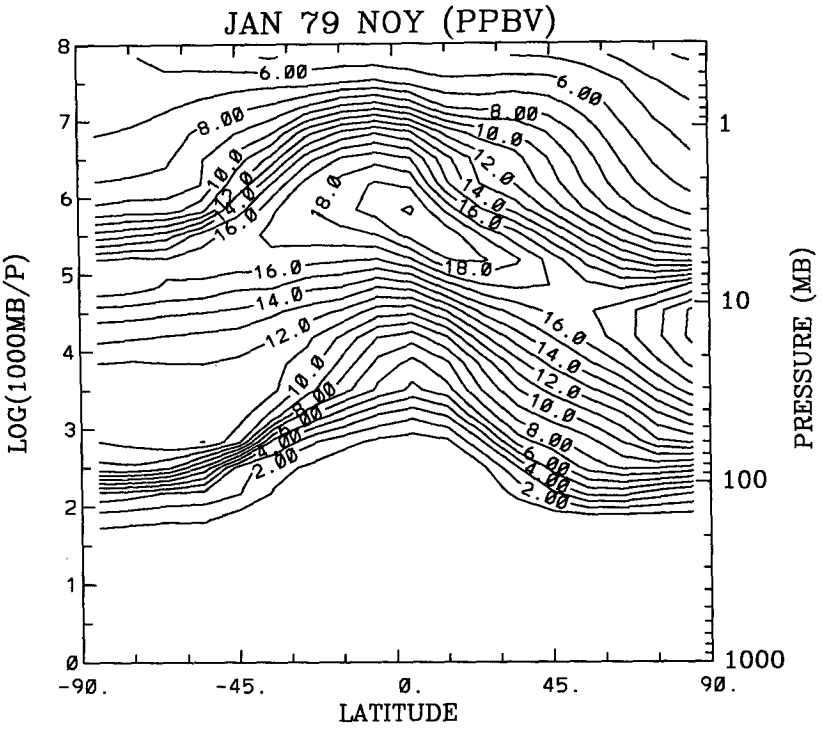

FIG. 12. Distribution of model simulated total odd nitrogen for January 1979.

NO_2

The correct simulation of ozone chemistry depends critically on our ability to simulate correctly the diurnal species NO_2, which dominates the catalytic loss of ozone in lower and middle stratosphere through the nitrogen cycle. Good simulation is achieved in our model, as can be seen by comparing LIMS and model daytime NO_2 for January 1979 in Fig. 15 (taken from Remsberg and Russell 1987) and Fig. 16.

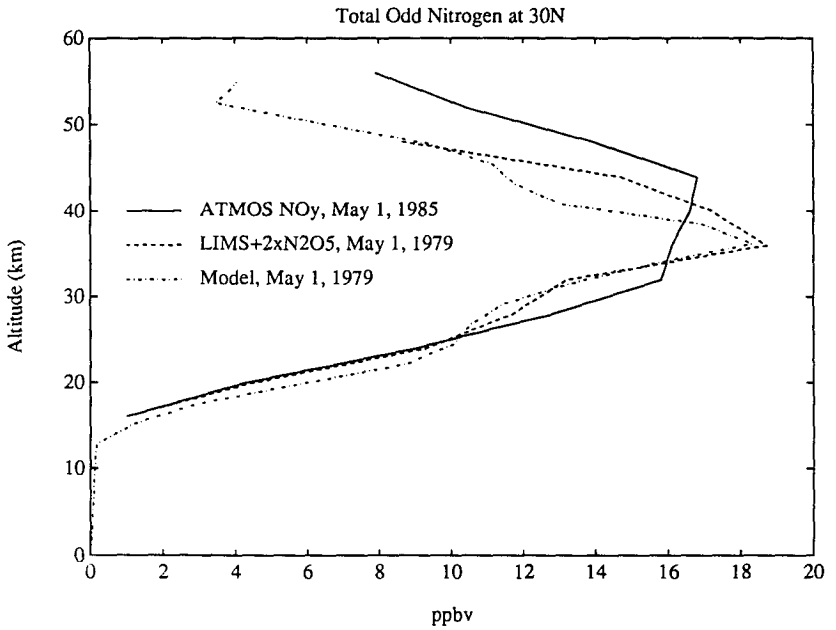

FIG. 13. Comparison of observed and model simulated vertical profile of total odd nitrogen at 30°N.

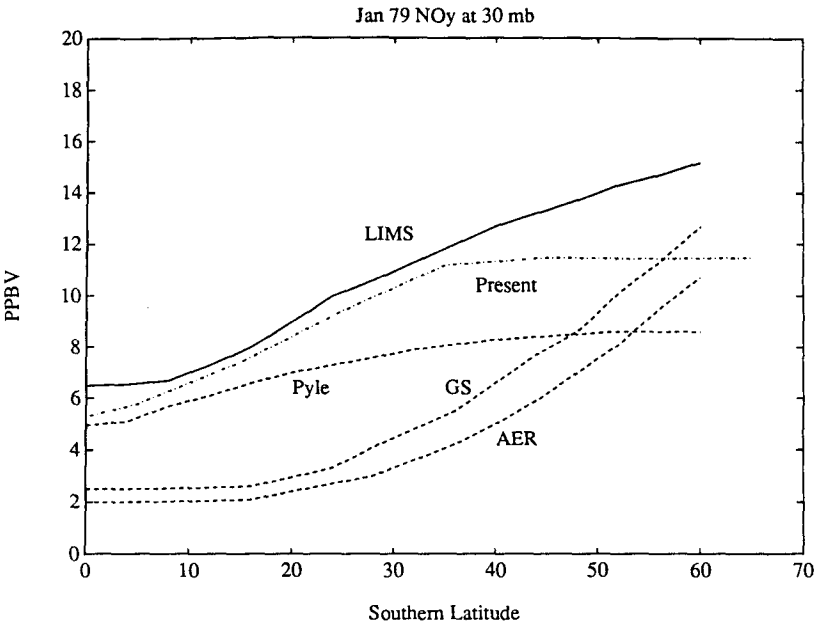

FIG. 14. Comparison of latitudinal distribution of total odd nitrogen between LIMS inferred data and various model results at 30 mb.

HNO_3

Nitric acid is observed to have very large latitudinal gradients (Gille et al. 1984); its column density varies by almost one order of magnitude from the equator to high latitudes. Many past attempts in simulating this latitudinal behavior have mostly failed, giving a U-shaped profile instead of the observed V-shape (see WMO 1986; Ko et al. 1985a, 1986).

In an earlier publication (Yang et al. 1990), we have suggested that the observed distribution of nitric acid, with low column values over the equator and high values at higher latitudes, can be simulated only if NO_y is transported with a latitudinally varying isentropic

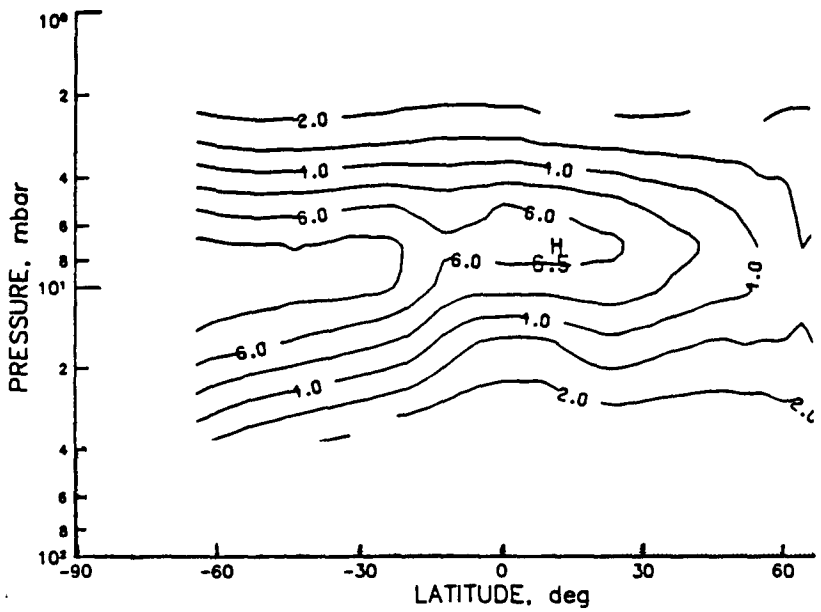

FIG. 15. LIMS daytime monthly zonal mean NO_2 cross section (ppbv) for January 1979 (taken from Remsberg and Russell 1987).

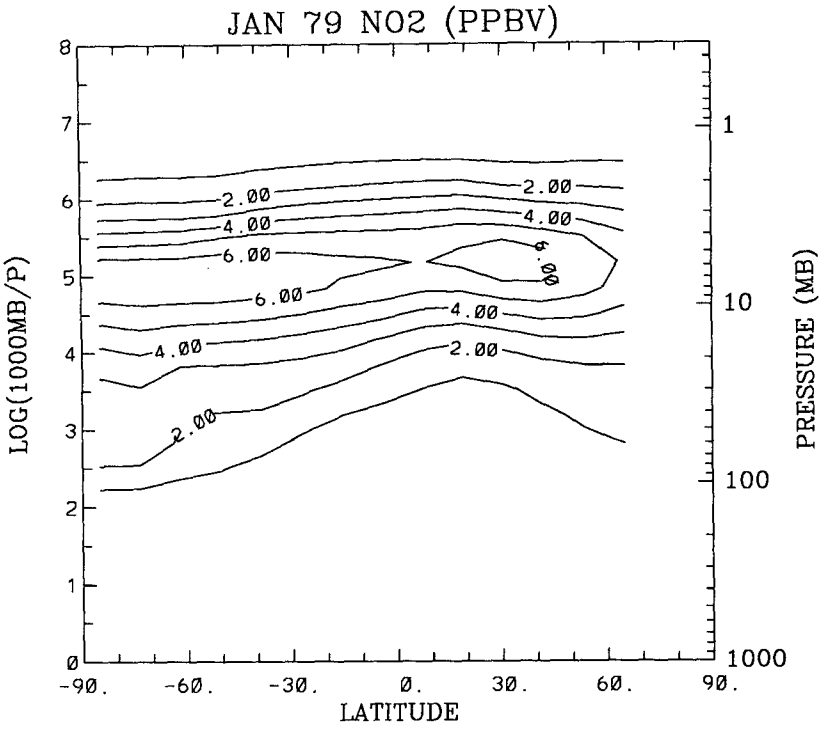

FIG. 16. Model simulated daytime monthly zonal mean NO_2 cross section (ppbv) for January 1979.

mixing coefficient K_{yy}, which is small over the tropics and large in the midlatitudes, and the associated diabatic circulation consistent with it, with an equatorial upwelling that is not too strong in the lower stratosphere. Such a K_{yy} and $\bar{Q}$ are what we have deduced from the observed mean temperature using a self-consistent formulation. A comparison of our simulated column density with LIMS observation (Gille et al. 1984) is given in Figs. 17 and 18 for May and December, respectively, when data are available.

Relative to earlier attempts with (uncoupled) model (see Ko et al. 1985a), the comparison of our result with observation is good in all sunlit (low to middle) latitudes. The V-shape is reproduced for the first time (see also Yang et al. 1990). The remaining discrepancy now occurs in the winter polar region. Since the life time of nitric acid becomes sufficiently long at high latitudes towards late fall and winter, it should not be treated as in photochemical equilibrium as was done in the present calculation (showing up in model Northern latitudes in the December comparison and also beginning to show up in May at high southern latitudes). In principle, such a problem can be overcome by transporting HNO_3 separately. Following Douglass et al. (1989), we have also performed such a calculation. In the absence of heterogeneous chemistry which is not incorporated in our model, HNO_3 behaves like a quasi-conservative tracer during polar night and is transported like other long-lived tracer by the model. The difference between the transported and non-transported version is small in low to middle latitudes. The transported version gives higher values

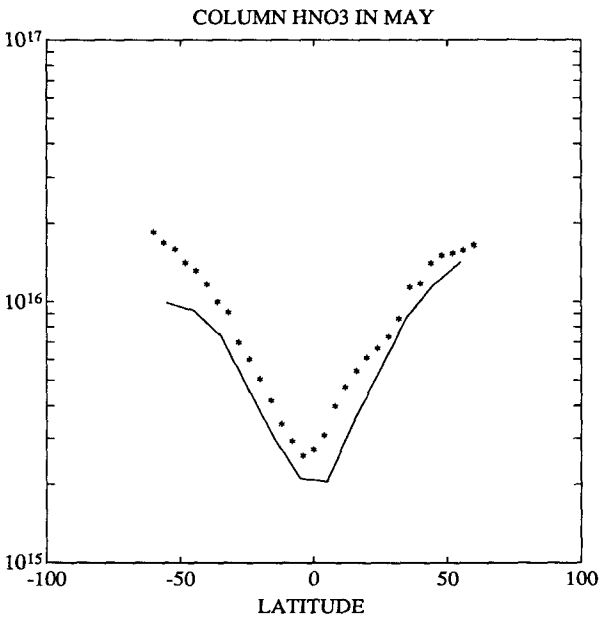

FIG. 17. Comparison of model simulated nitric acid column density with LIMS observation (Gill et al. 1984) for the month of May, 1979. Observation is shown in solid line.

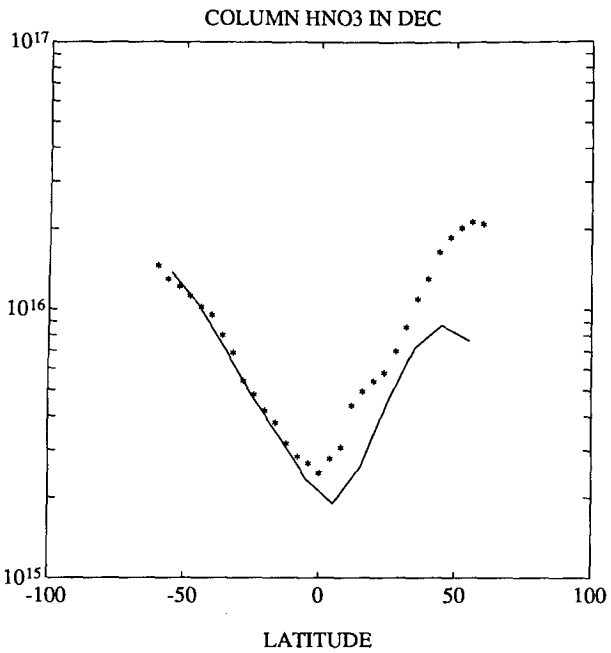

FIG. 18. Same as Fig. 17, except for December. Observation is for 1978, model data is for 1979.

during polar night at high latitudes than the version which assumes photochemical equilibrium. The comparison has been given by Douglass et al. (1989) and so will not be shown here. It should be pointed out, additionally, that both versions of the model yield winter values that are still smaller than the observed data poleward of 55°N in winter; the latter shows HNO_3 increasing sharply with latitude inside the polar vortex, suggesting perhaps that night time heterogeneous chemistry that converts N_2O_5 to nitric acid may become important at these times and latitudes as was shown by Austin et al. (1986).

Since no heterogeneous chemistry is included in the present model, comparison with observations for the equinoxial months may be more meaningful than solsticial months. In Fig. 19, taken from WMO (1986) report, LIMS HNO_3 data for the month of April of 1979 is shown. The corresponding result from our model is presented in Fig. 20. Favorable comparison is found in the low to middle latitudes. The south polar values are too low in the model; this is to be expected since the assumption of photochemical equilibrium breaks down there.

A further comment concerning the transported versus nontransported version of HNO_3 in the sunlit region should be added. From a strictly numerical point of view, it is preferable to include nitric acid within the reactive nitrogen family in a 2-D model. Since the net production of nitric acid in sunlit regions is equal to the small difference between competing production and loss terms, any errors in the computation of the individual terms will result in much larger relative errors in the net photochemical generation rate. The transported version is much more sensitive to numerical resolution and other uncertainties in the production and loss rates of HNO_3, and hence also in the production and loss rates of NO_y (with HNO_3 removed). Such a problem does not show up when HNO_3 is included in the definition of NO_y in the family approximation. To do the problem correctly with HNO_3 transported separately, high vertical resolution (<1 km) is needed. At 1 km resolution, our model results show very little difference between the transported and nontransported versions in the low and middle latitudes. At 2 km resolution, the nontransported version is close to the results at 1 km resolution,

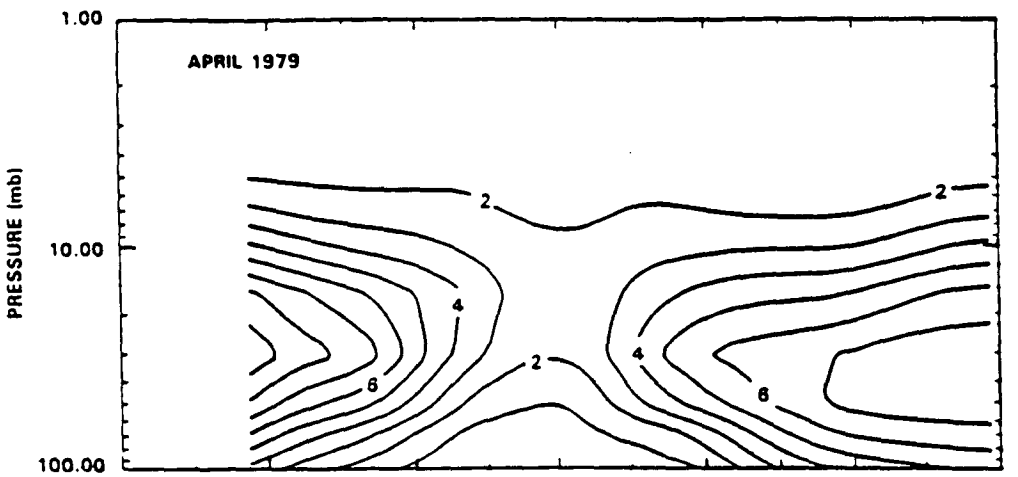

FIG. 19. Monthly averaged zonal mean cross section of HNO_3 mixing ration (ppbv) from LIMS for April 1979 (taken from WMO 1986).

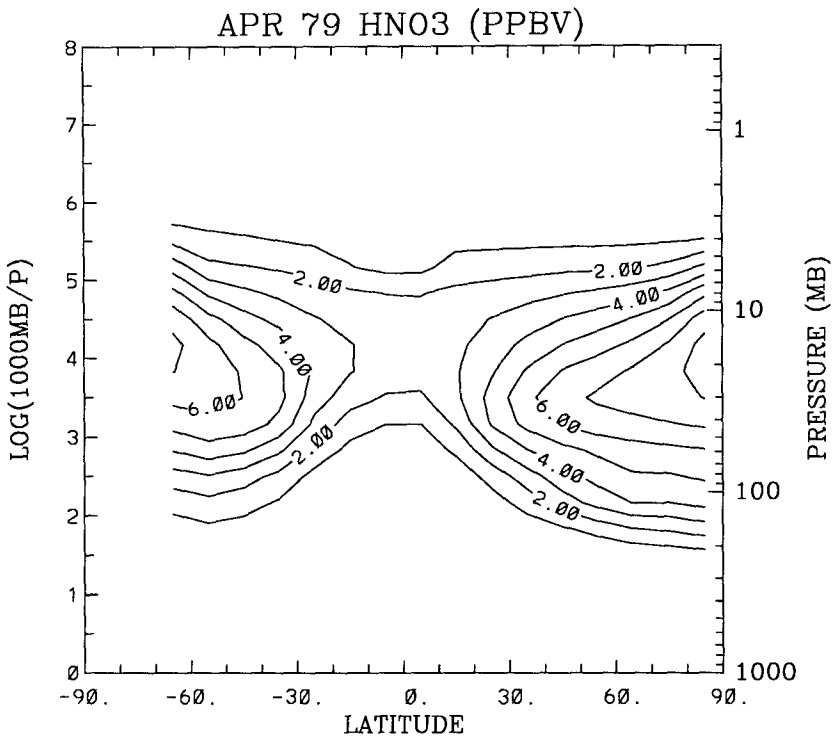

FIG. 20. Model-simulated monthly averaged zonal mean cross section of HNO_3 mixing ration for April 1979.

but the transported version at 2 km is very different from that at 1 km.

Our model calculation, with only gas phase chemistry, does not appear to have significant problems during the summer, although the summer model values of column nitric acid have been found by other groups to be systematically too high when compared with LIMS data.

Therefore, previously known model discrepancies concerning HNO_3 column amount appear to have been largely overcome with our present model, except systematically during winter and late fall at high latitudes (in both hemispheres) where daylight hours are short, and where nighttime heterogeneous reactions may become important.

9. Methane and nitrous oxide

CH_4

Both CH_4 and N_2O are long-lived species with surface sources and well mixed tropospheric concentrations. Both decrease with altitude in the stratosphere due to photochemical sinks. Because of their small horizontal gradients, these species are not as sensitive to the treatment of horizontal diffusion (K_{yy}) as is HNO_3, for example, but are quite sensitive to the vertical advective and diffusive transports as far as the tracer slopes are concerned (Guthrie et al. 1984; Ko et al. 1985a).

Monthly mean cross sections of CH_4 between 50°S and 70°N for 1979 as measured by the Nimbus 7 SAMS instrument is shown in Fig. 21 (taken from Jones and Pyle 1984). Our model simulation for the same periods is shown in Fig. 22. The agreement between model and observation can be considered as excellent for the months of January and July. Note in particular the tilting of the isopleths towards the summer hemisphere, with the "bump" located near 20° in the Southern Hemisphere in January and Northern Hemisphere in July. This feature is due to the direction of the diabatic circulation (Solomon et al. 1986), which is rising in the summer hemisphere and sinking in the winter hemisphere. The upwelling portion, which is responsible for bringing up air with high methane concentrations, is located closer to the equator in the lower stratosphere, shifting to higher summer latitudes with height. This accounts for the tilt.

The simulation for April is deficient in the equatorial upper stratosphere. The observed double peak in the tracer isopleths is not simulated. It was suggested (Solomon et al. 1986) that this feature was caused by locally warm temperatures associated with the semiannual oscillation occurring in the equatorial upper stratosphere.

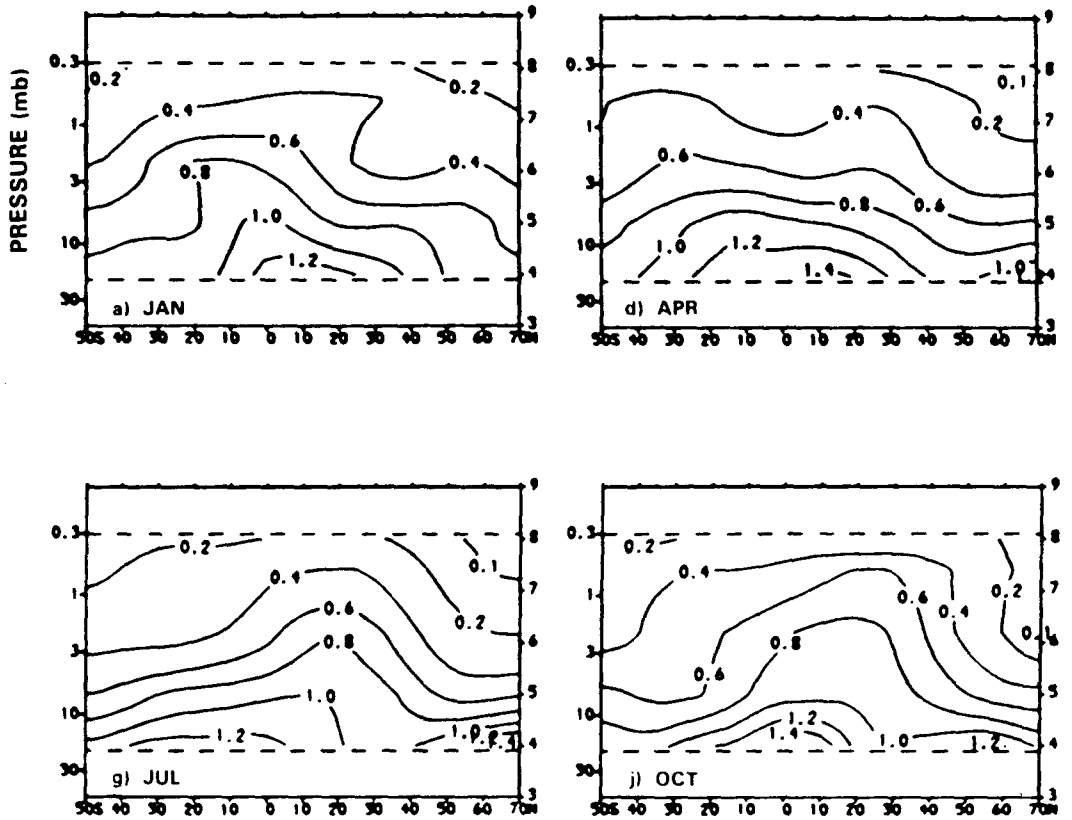

FIG. 21. Monthly mean cross section of CH_4 (ppmv) for 1979 measured by the Nimbus 7 SAMS (taken from Jones and Pyle 1984).

Although our model net heating rate does show a negative departure from radiative equilibrium ($\bar{Q} < 0$) at the right location (Yang et al. 1990), which gives a local subsidence (see Fig. 1), the calculated subsidence is apparently not strong enough to bring down enough low values of CH_4 to yield a noticeable double peak. The data quality at this altitude for the NMC temperatures adopted here may be suspect.

N_2O

The monthly mean cross sections of N_2O between 50°S and 70°N as measured by SAMS for 1979 is shown in Fig. 23, while our model result for the same period is shown in Fig. 24. Except for the absence of the double peak feature in April in the equatorial upper stratosphere, the comparison is very favorable. Both the observed and model simulated N_2O behave strikingly similar to those of CH_4, a fact anticipated on theoretical grounds (WMO 1986; Plumb and McConalogue 1988). We do not seem to have the problem, encountered by Solomon et al. (1986), of model overestimating the abundance of N_2O at tropical latitudes while underestimating the CH_4 mixing ratios. Jones and Pyle (1984) also found overestimated N_2O abundance in the model as compared to SAMS.

Except near the top of the model domain, all N_2O mixing ratio isopleths with values 200 ppbv or less are very close to LIMS contours. Near the lower altitude limit of LIMS, a 300 ppbv contour appears to be present in LIMS, but not in our model. Because of the uncertainty of LIMS at such low altitudes, it is not known if such a steep vertical gradient as implied by LIMS near 20 mb is real and should be taken to indicate a model deficiency.

Near the top of the model domain, both N_2O and CH_4, and also O_3 mentioned earlier, show systematically lower values than the observed. This feature will be discussed again later.

10. The chlorofluorocarbons and active chlorines

CFCs are man-made chlorine-containing compounds. Upon their release into the troposphere, CFCs are transported into the stratosphere where they are photochemically decomposed, releasing chlorine atoms which destroy ozone through a catalytic cycle of chemical reactions. A correct simulation of their distribu-

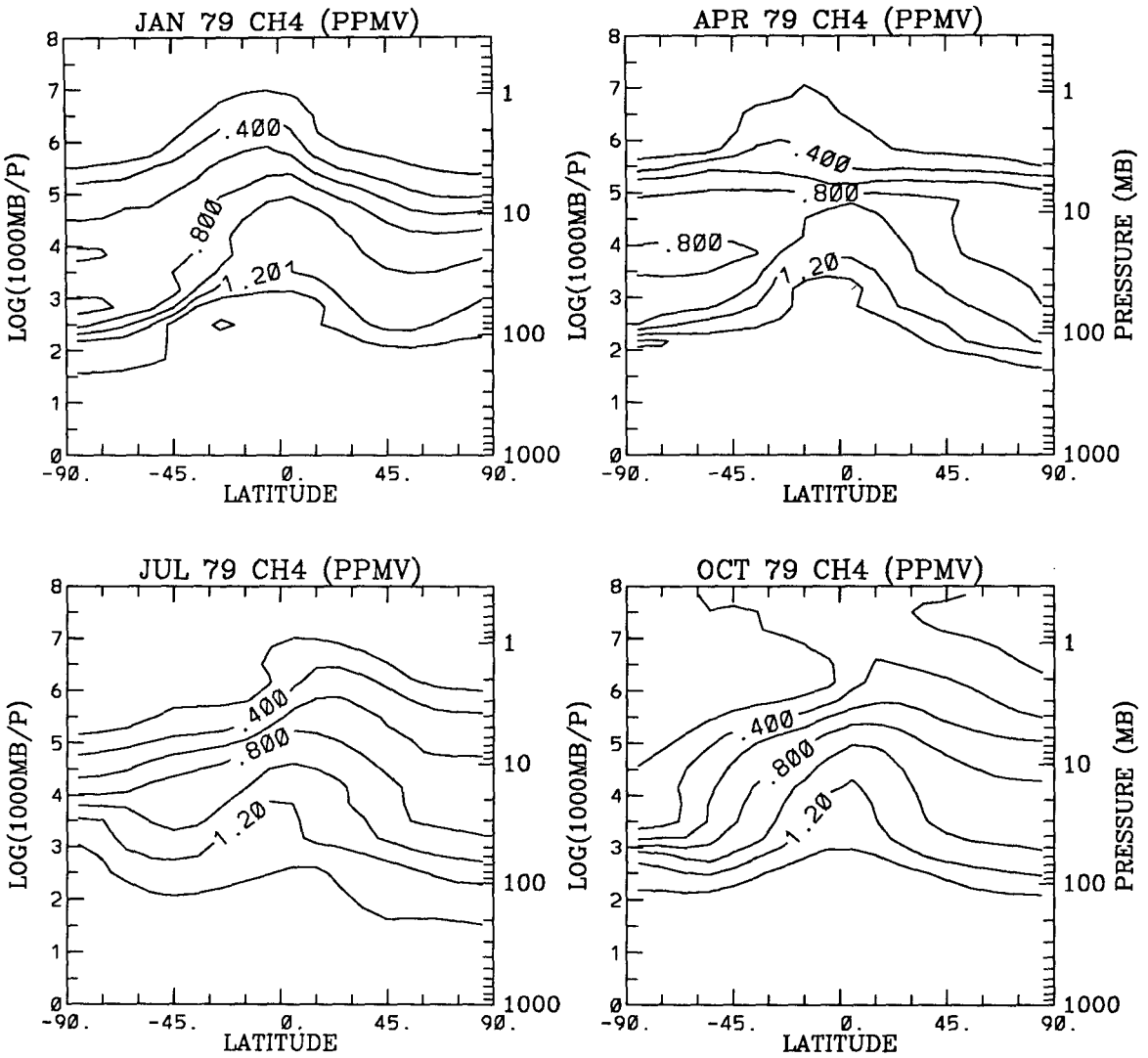

FIG. 22. Model simulated monthly mean cross section of CH_4 (ppmv) for 1979.

tions would provide us with further evidence supporting the model transport parameters, as well as our understanding of their photochemistry, as a first step toward reliable prediction of future ozone depletion by CFCs.

In Fig. 25, we plot three model simulated CFC species, F10, F11, and F12, at 45°N for 1 October 1980, along with observations made in 1982 and 1983, taken from WMO (1986). It shows quite satisfactory agreement between the simulated and the observed profiles, both exhibiting sharp vertical gradients in lower stratosphere, which is a result of photochemical decomposition of CFCs there.

The resulting total amount of chlorine generated by our model is shown in Fig. 26, which shows Cl_y values ranging from 2.0 to 2.2 ppbv in the stratosphere. These values are in agreement with observations (Berg et al. 1980; Gallagher et al. 1985), perhaps in the lower end of the more recently observed range, partially due to our use of 1980 boundary conditions for CFCs. Other 2-D models yield upper stratospheric Cl_y values ranging from 1.8 to 2.5 ppbv (see WMO 1986).

11. Discussion of systematic trends

From a scientific point of view, one of the advantages of attempting to simulate a large number of chemical species simultaneously is the possibility that a *systematic* agreement with, or discrepancy from, observation can be discerned. We are aided in this process by the recent availability of satellite data for many species covering most of the globe and all seasons. By com-

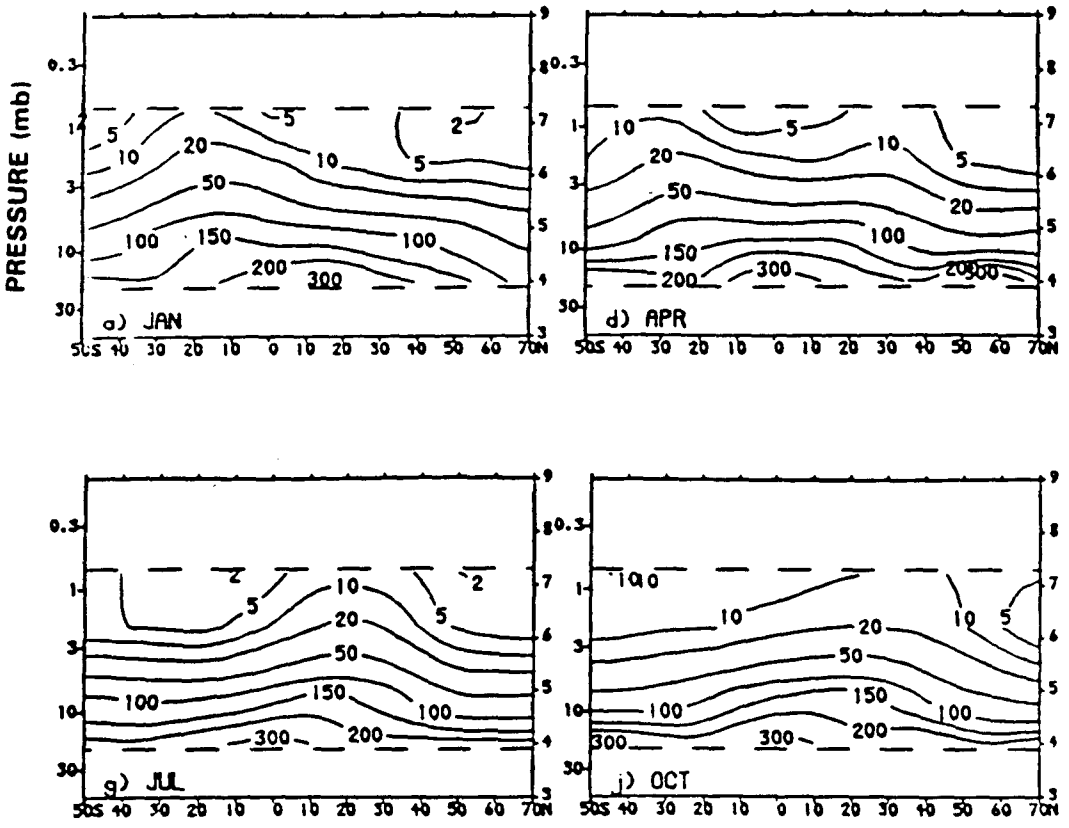

FIG. 23. Monthly mean cross section of N_2O (ppbv) for 1979 measured by the Nimbus 7 SAMS (taken from Jones and Pyle 1984).

paring with this dataset and with previous model results, we have noticed a number of systematic improvements over previous model results and a systematic deficiency.

Ko et al. (1984) performed a similar experiment using a classical Eulerian 2-D model. Although there were many empirical, and hence tunable, parameters in that generation of models, no attempt was made to adjust the parameters to obtain better agreement with data. Instead their expressed goal was to "look for systematic agreements and discrepancies between model and observation for a wide range of species." One major systematic discrepancy noted by Ko et al. (1984) was that "at the equatorial region, the model tends to underestimate the concentrations of upward diffusing species (e.g., CFCs, CH_4, N_2O) and overestimate the column abundances of the downward diffusing species (HNO_3, HCl, O_3)[2]."

[2] The "upward/downward diffusing species" are referred to by chemists to mean those species that have their sources in the troposphere/stratosphere and are transported to other parts of the atmosphere by both advective and diffusive transports. The terms "upward/downward diffusing" are more appropriate for 1-D chemical models in which vertical diffusion is the only mode of dynamical transport.

The above-quoted systematic discrepancy can be interpreted as an indication that the classical Eulerian model was too diffusive, resulting in too small a latitudinal gradient and hence an underestimate of the abundance of upward diffusing species and an overestimate of the column abundance of downward diffusing species in the equatorial region. This is one of the factors that motivated the switch over into the so-called diabatic circulation or residual circulation models (Guthrie et al. 1984; Ko et al. 1985a, Garcia and Solomon 1983; Stordal et al. 1985).

In the newer, and more physically based, version, the tracer slopes were no longer determined by the hypothetical "mixing paths", whose direction and orientation are given by the relative magnitudes of the different components of the diffusion tensor. Instead, meridional gradients of tracer concentrations are created on surfaces of constant potential temperature by differential diabatic heating or cooling ($\bar{Q}$) and smoothed by large-scale diffusive mixing acting predominantly along the isentropic surfaces (Mahlman et al. 1984; Tung 1982, 1984). It was argued (Tung 1984; Ko et al. 1985a) that perhaps a lower value of K_{yy} should be used in this second generation of models. A value of $K_{yy} = 3 \times 10^9$ cm^2 s^{-1} was adopted by several groups. A systematic improvement in the latitudinal

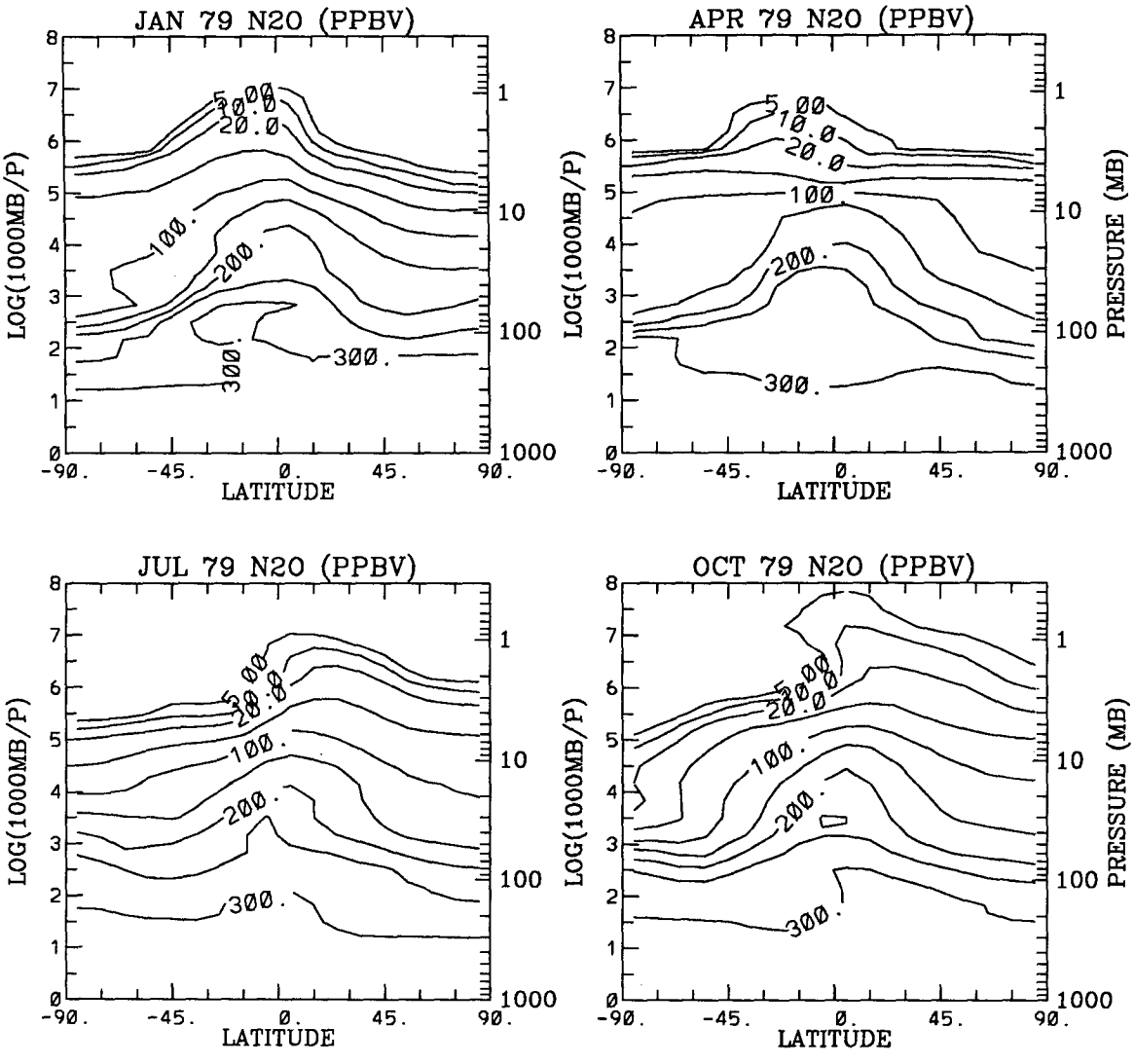

FIG. 24. Model simulated monthly mean cross section of N_2O (ppbv) for 1979.

and seasonal gradients of many species was noted. The work of Guthrie et al. (1984), Ko et al. (1985a) and Solomon and Garcia (1984) further yielded circumstantial evidence that vertical mixing should be very small in the bulk of the stratosphere, in support of the assumption of wave mixing occurring predominantly along isentropic surfaces.

Despite the improvement over earlier models, some notable discrepancies remained when compared with available data. These discrepancies appeared to be *common* among most 2-D models of similar formulation, but a *systematic* trend was difficult to discern. It was not clear whether the discrepancies, such as the equatorial NO_y deficit problem, should be attributed to model formulation or to missing chemical sources.

We suggest here that many of the remaining model deficiencies can be removed with a further refinement of model formulation and implementation. In particular, the momentum equations should be used to relate the diffusion coefficient K_{yy} to the observed zonal mean momentum budget, and a more comprehensive radiative transfer calculation should be done especially in the region of equatorial lower stratosphere. More importantly, the advective and diffusive transports should be consistent with each other (Plumb and Mahlman 1987; Newman et al. 1986) and the latter should have important latitudinal and seasonal variations. In particular, the K_{yy} value should be small (about 1×10^9 cm^2 s^{-1}) in the tropics and over the poles and large (about 5×10^9 cm^2 s^{-1}) over the middle latitudes. Implementation of these ideas yielded our present version of the model, with (almost) no tunable parameters.

Systematic improvement over previous generations of 2-D model is attributed to the following factors:

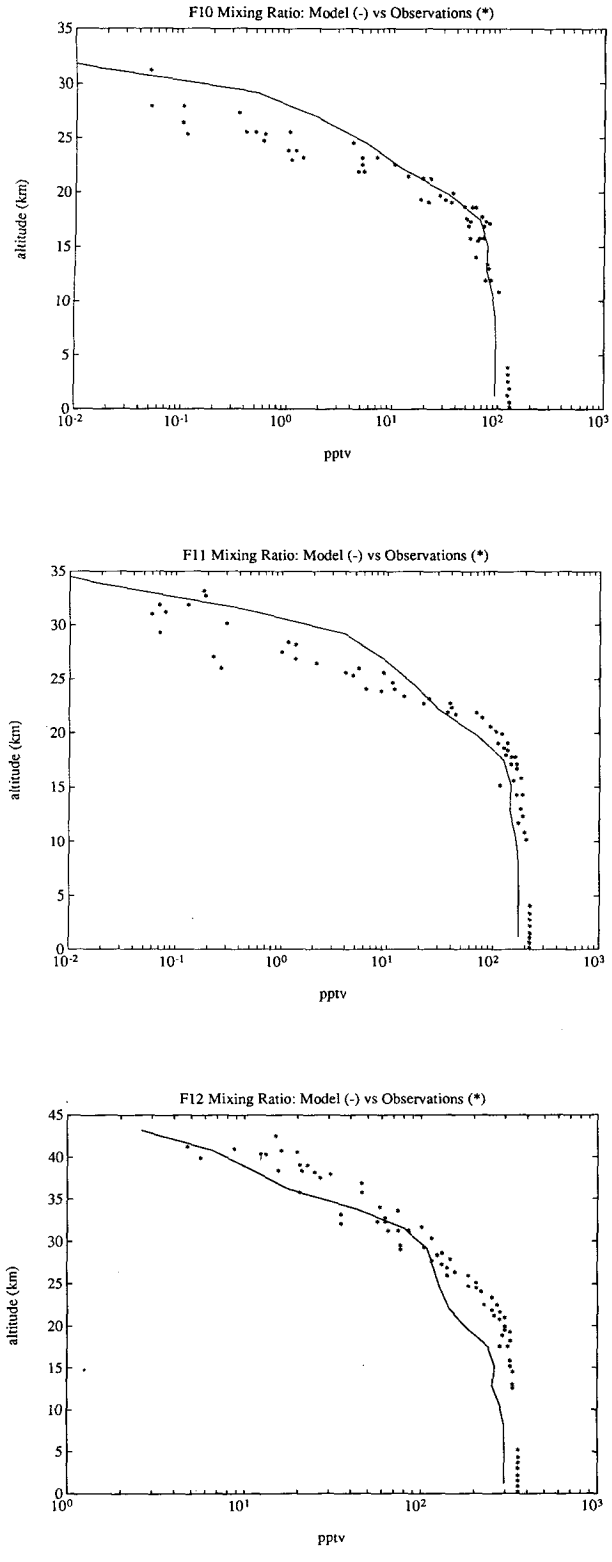

FIG. 25. Comparison of model simulated CFCs at 45°N for 1 October 1980 with observations (from WMO 1986) made during 1980 to 1983 (a) for F10, (b) for F11 and (c) for F12.

1) The diabatic heating used in most previous models is probably too strong in the equatorial lower stratosphere. It is well known that the diabatic heating of this region is particularly difficult to assess, owing to the delicate balance among several competing terms. The most difficult contribution to compute among these terms is the heating due to ozone absorption in the 9.6 μm band, which is often overestimated in models (Crisp 1989). Additionally, although we demonstrate in another paper (Olaguer et al. 1990) that the *net* effect of clouds is small, many groups retain only the visible albedo effect of clouds without also including the compensating effect of IR cooling of clouds, thus contributing to an overestimate of the heating in the lower stratosphere. We found that the combined effect of these two errors can be as high as 0.3 K day^{-1} at around 25 km in the tropics, compared to a net heating of about 0.2 K day^{-1} as computed by a more accurate model using satellite observations of temperature and absorbers as input (see Olaguer et al. 1990). This value is lower than the value from Dopplick (1979) used in some 2-D models by a factor of 2.

An overly positive net diabatic heating in the tropics implies a strong equatorial upwelling, which in turn leads to a deficit of odd nitrogen and an overestimate of N_2O mixing ratios in the stratosphere. However, since advective transport is but one of the many factors affecting the concentration of a chemical species such as NO_y, one cannot conclude that the deficit of the model NO_y necessarily implies that the upwelling is too strong. In this regard, model calibration using inert tracers is extremely useful. Shia et al. (1989) performed a series of experiments using ^{14}C as a tracer to gauge the appropriateness of model transport parameters for the lower stratosphere. Some models were found to have equatorial upwelling that was up to a factor of three too strong. Ours were found to be approximately consistent with data.

2) The isentropic mixing coefficient K_{yy} should be smaller in the equatorial region and larger in the mid-latitude region than the constant value used previously. The observed latitudinal profile of nitric column appears to indicate that such a feature for K_{yy} is necessary (see also Yang et al. 1990). For ozone, more horizontal mixing from the subtropical to equatorial regions takes place in earlier models compared to ours. The resulting higher equatorial column ozone was "tuned down" in some models by adjusting the equatorial upwelling, making it even *stronger*, and causing an even more serious deficit in the total odd nitrogen.

A systematic deficiency in our model appears to occur near and above 40 km. The model vertical gradients for N_2O, CH_4 and NO_y appear to be steeper than the observed and the O_3 values at 40 km are too low com-

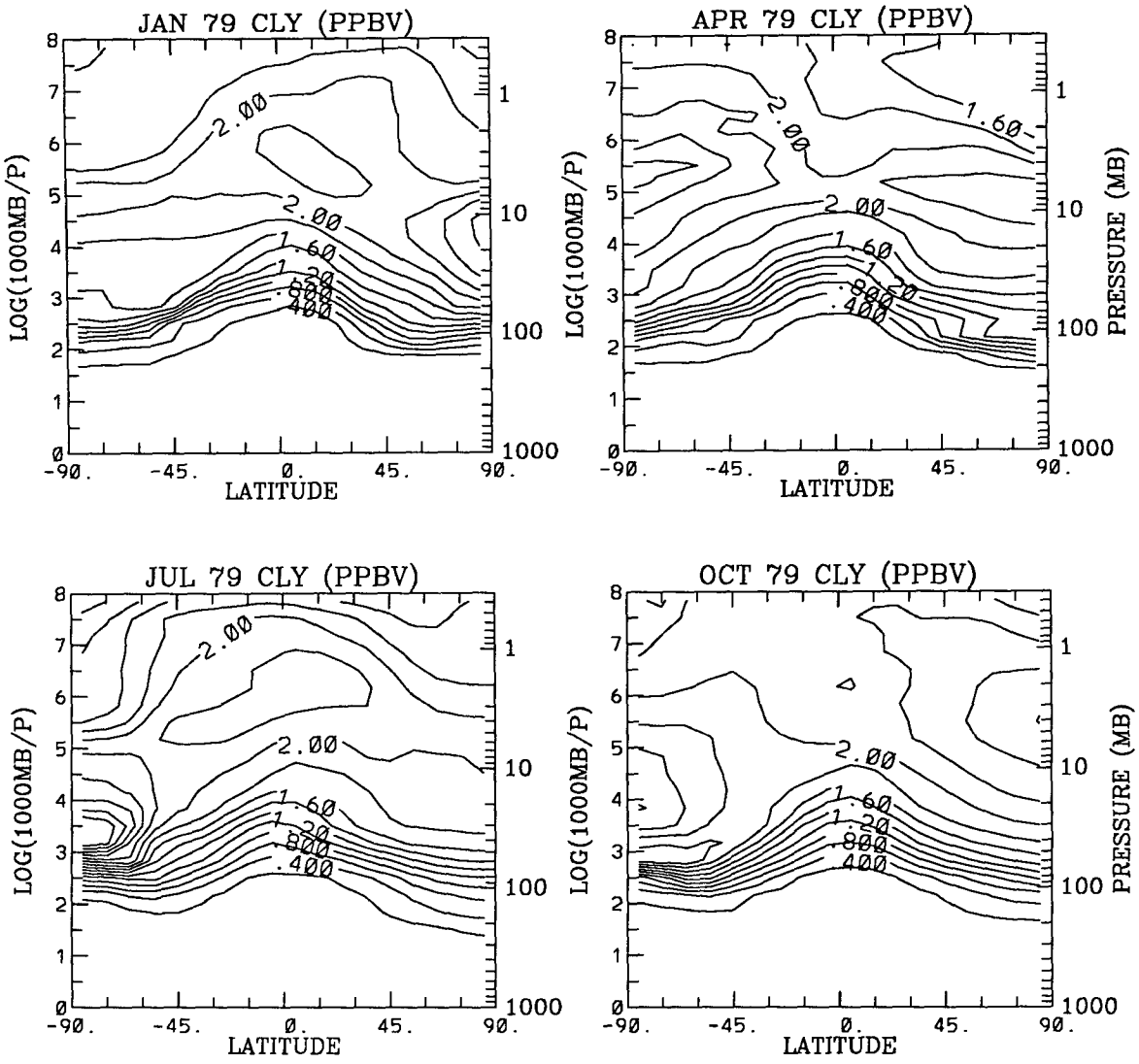

FIG. 26. Model simulated monthly mean cross section of Cl_y (ppbv) for 1979.

pared with the SBUV values. It is possible that, at least for N_2O, CH_4 and NO_y, these are due to a lack of gravity wave vertical mixing in the model. Nevertheless, below 35 km where the bulk of ozone resides, our assumption of planetary wave mixing along isentropic surfaces appears to be correct.

Acknowledgments. Helpful conversations with Professor Yuk L. Yung of Caltech and Dr. Charles Jackman of NASA Goddard are gratefully acknowledged. The research is supported by NASA, under Grants NAGW-910 and NAGW-1605, and by NSF, under Grant ATM8903340. Helpful comments by two reviewers, and by editor Rolando Garcia are gratefully acknowledged.

APPENDIX A

Summary of Photochemical Scheme

A. Specify:

$$[H_2]/[M] = 0.5 \text{ ppm}$$

$$[O_2] = 0.21[M]$$

$$[N_2] = 0.78[M].$$

B. Predict $[O_x] = [O(^1D)] + [O] + [O_3]$ from ($[X]_t$ means $d[X]/dt$):

$$[O_x]_t = 2J_1[O_2] - 2k_4[O][O_3] - 2l_6[M][O]^2 + 2k_{41}[NO][HO_2] - 2l_{69}[M][ClO]^2$$

$$- k_{23}[CO][OH] - 2(k_{27}[OH] + k_{44}[NO_2] + k_{58}[ClO])[O] - 2\{k_{26}[OH] + k_{45}[NO_2]J_{47}/(J_{46} + J_{47})\}[O_3]$$

$$\frac{[O(^1D)]}{[O_3]} = \frac{J_2}{k_7[N_2] + k_8[O_2]}$$

$$\frac{[O]}{[O_3]} = \frac{J_2 + J_3}{l_5[M][O_2]}.$$

C. Predict CH_4, CO, N_2O, NO_y, CFCs, Cl_y, H_2O and HF: ($[X]_t$ means $d[X]/dt$):

$$[CH_4]_t = -\{k_{12}[O(^1D)] + k_{13}[OH] + k_{60}[Cl]\}[CH_4]$$

$$[CO]_t = -[CH_4]_t - k_{23}[OH][CO]$$

$$[N_2O]_t = -\{(k_{35} + k_{36})[O(^1D)] + J_{37}\}[N_2O]$$

$$[NO_y]_t = 2k_{35}[N_2O][O(^1D)] - 2k_{38}[N][NO]$$

$$[CCl_4]_t = -J_{72}[CCl_4]$$

$$[CFCl_3]_t = -J_{73}[CFCl_3]$$

$$[CF_2Cl_2]_t = -J_{74}[CF_2Cl_2]$$

$$[CH_3CCl_3]_t = -(J_{75} + k_{76}[OH])[CH_3CCl_3]$$

$$[CH_3Cl]_t = -(J_{77} + k_{78}[OH])[CH_3Cl]$$

$$[CClF_2CCl_2F]_t = -J_{79}[CClF_2CCl_2F]$$

$$[CHClF_2]_t = -(J_{80} + k_{81}[OH])[CHClF_2]$$

$$[Cl_y]_t = -4[CCl_4]_t - 3[CFCl_3]_t - 2[CF_2Cl_2]_t - 3[CH_3CCl_3]_t - [CH_3Cl]_t - 3[CClF_2CCl_2F]_t - [CHClF_2]_t$$

$$[H_2O]_t = \{k_{13}[CH_4] + k_{16}[CH_3OOH] + k_{19}[CH_2O] + k_{24}[HO_2] + k_{33}[H_2O_2] + k_{50}[HNO_3] + k_{52}[HNO_4] + k_{65}[HOCl]\} \times [OH] - (J_9 + k_{10}[O(^1D)])[H_2O]$$

$$[HF]_t = J_{73}[CFCl_3] + 2J_{74}[CF_2Cl_2] + 3J_{79}[CClF_2CCl_2F] + 2(J_{80} + k_{81}[OH])[CHClF_2].$$

D. Deduce NO_y species:

$$\frac{[NO]}{[NO_2]} = \frac{J_{42} + k_{44}[O] + k_{45}J_{47}/(J_{46} + J_{47})[O_3]}{k_{17}[CH_3O_2] + k_{41}[HO_2] + k_{43}[O_3] + k_{59}[ClO]}$$

$$\frac{[N]}{[NO]} = \frac{J_{39}}{k_{40}[O_2]}$$

$$\frac{[NO_3]}{[NO_2]} = \frac{k_{45}[O_3]}{J_{46} + J_{47}}$$

$$\frac{[HNO_3]}{[NO_2]} = \frac{l_{48}[M][OH]}{J_{49} + k_{50}[OH]}$$

$$\frac{[HNO_4]}{[NO_2]} = \frac{l_{51}[M][HO_2]}{J_{53} + k_{52}[OH]}$$

$$\frac{[ClONO_2]}{[NO_2]} = \frac{l_{66}[M][ClO]}{J_{67} + k_{68}[O]}$$

$$[N_2O_5]_{DTA} = \frac{1 - \exp(-2k_{45}[O_3]T_N)}{2(J_{55} + j_{56})_{DTA}T_D} \times ([NO] + [NO_2])_{DTA}$$

$$[NO_2] = [NO_y]\Big/\left(1 + \frac{[N]}{[NO_2]} + \frac{[NO]}{[NO_2]} + \frac{[NO_3]}{[NO_2]} + \frac{[HNO_3]}{[NO_2]} + \frac{[HNO_4]}{[NO_2]} + \frac{[ClONO_2]}{[NO_2]} + \frac{2[N_2O_5]}{[NO_2]}\right)$$

where $[X]_{DTA}$ means day-time average of $[X]$, T_N and T_D are the nighttime length and daytime length, respectively. A brief derivation of the daytime average concentration of N_2O_5 is given below.

The N_2O_5 balance is obtained by assuming that reactions 45, 54 and 56 occur at night resulting in the build-up of N_2O_5, which is then destroyed by photodissociation (reaction 55) and thermal decomposition (reaction 56) during the day. We ignore the depletion of NO_2 by reaction 66, since ClO is much more rapidly depleted during the night in the lower stratosphere. NO_3 is assumed to be in equilibrium, so that the only members of the NO_y family whose concentrations change with time due to photochemical processes are NO_2 and N_2O_5. Night time chemistry can then be expressed in terms of the following coupled system of differential equations:

$$[N_2O_5]_t = k_{45}[O_3][NO_2]$$

$$[NO_2]_t = -2k_{45}[O_3][NO_2].$$

Solving this system analytically yields the amount of N_2O_5 present at the end of the night:

$$[N_2O_5]_{dawn} = [N_2O_5]_{dusk} + 0.5[NO_2]_{dusk} \times [1 - \exp(-2k_{45}[O_3]T_N)].$$

The dusk concentration of NO_2 is equal to the sum of the daytime-average concentrations of NO and NO_2. The N_2O_5 concentration at the end of the daytime is in turn given by

$$[N_2O]_{dusk} = [N_2O_5]_{dawn} \exp[-(J_{55} + j_{56})T_D].$$

Combining the previous two equations yields the expression for $[N_2O_5]_{DTA}$ given above.

E. Deduce HO_x species:

$$\frac{[H]}{[OH]} = \frac{k_{23}[CO] + k_{27}[O]}{k_{28}[O_3] + l_{29}[M][O_2]}$$

$$\frac{[HO_2]}{[OH]} = \frac{k_{26}[O_3] + l_{29}[M][O_2][H]/[OH]}{k_{30}[O] + k_{31}[O_3] + k_{41}[NO] + k_{63}[ClO]}$$

$$[H_2O_2] = \frac{k_{32}[HO_2]^2}{k_{33}[OH] + J_{34}}$$

$$(k_{33}[H_2O_2] + k_{50}[HNO_3] + k_{52}[HNO_4] + k_{62}[HCl] + k_{65}[HOCl])[OH] + (k_{24}[OH] + k_{25}[H])[HO_2] - (J_9 + k_{10}[O(^1D)])[H_2O] - k_{11}[O(^1D)][H_2] - J_{20}[CH_2O] - (k_{12}[O(^1D)] + k_{60}[Cl])[CH_4] = 0.$$

F. Deduce hydrocarbon species:

$$[CH_2O] = \frac{-[CH_4]_t}{k_{19}[OH] + J_{20} + J_{21}}$$

$$[CH_3O_2] = \frac{-[CH_4]_t}{k_{17}[NO]}$$

$$[CH_3OOH] = \frac{k_{15}[CH_3O_2][HO_2]}{k_{16}[OH]}.$$

G. Deduce Cl_y species:

$$\frac{[ClO]}{[Cl]} = \frac{k_{57}[O_3]}{k_{58}[O] + k_{59}[NO] + k_{63}[HO_2] + 2l_{69}[M][ClO]}$$

$$\frac{[HCl]}{[Cl]} = \frac{k_{60}[CH_4] + k_{61}[HO_2]}{k_{62}[OH]}$$

$$\frac{[HOCl]}{[ClO]} = \frac{k_{63}[HO_2]}{J_{64} + k_{65}[OH]}$$

$$\frac{[ClONO_2]}{[ClO]} = \frac{l_{66}[M][NO_2]}{J_{67} + k_{68}[O]}$$

$$[ClO] = \frac{[Cl_y]}{1 + \frac{[Cl]}{[ClO]} + \frac{[HCl]}{[ClO]} + \frac{[HOCl]}{[ClO]} + \frac{[ClONO_2]}{[ClO]}}.$$

REFERENCES

Allen, M., and J. E. Frederick, 1982: Effective photodissociation cross sections for molecular oxygen and nitric oxide in the Schumann–Runge bands. *J. Atmos. Sci.*, **39**, 2066–2075.

Austin, J., R. R. Garcia, J. M. Russell III, S. Solomon and A. F. Tuck, 1986: On the atmospheric photochemistry of nitric acid. *J. Geophys. Res.*, **91**, 5477–5485.

Baulch, D. L., R. A. Cox, P. J. Crutzen, R. F. Hampson, J. A. Herr, J. Troe and R. T. Watson, 1982: Evaluated kinetic and photochemical data for atmospheric chemistry: Supplement I. CODATA Task Group on Chemical Kinetics. *J. Phys. Chem. Ref. Data*, **11**, 327–496.

Berg, W. W., P. J. Crutzen, F. E. Grahek, S. N. Gitlen and W. A. Sedlacek, 1980: First measurements of total chlorine and bromine in the lower stratosphere. *Geophys. Res. Lett.*, **7**, 937–940.

Brasseur, G., M. H. Hitchman, S. Walters, M. Dymek, E. Falise and M. Pirre, 1990: An interactive chemical dynamical radiative two-dimensional model of the middle atmosphere. *J. Geophys. Res.*, **95**, 5639–5655.

Crisp, D., S. B. Fels and M. D. Schwarzkopf, 1986: Approximate methods for finding CO2 15-micron band transmission in planetary atmospheres. *J. Geophys. Res.*, **91**, 11 851–11 866.

——, 1989: Comparison of thermal infrared cooling rates. Two-dimensional intercomparison of stratospheric models. NASA Conf. Pub. 3042, 89–107.

Cunnold, D., F. Alyea, N. Phillips and R. Prinn, 1975: A three-dimensional dynamical-chemical model of atmospheric ozone. *J. Atmos. Sci.*, **32**, 170–194.

Donner, L., and V. Ramanathan, 1980: Methane and nitrous oxide: Their effects on the terrestrial climate. *J. Atmos. Sci.*, **43**, 119–124.

Dopplick, T. G., 1972: Radiative heating of the global atmosphere. *J. Atmos. Sci.*, **29**, 1278–1294.

——, 1979: Radiative heating of the global atmosphere: Corrigendum. *J. Atmos. Sci.*, **36**, 1812–1817.

Douglass, A. R., C. H. Jackman and R. S. Stolarski, 1989: Comparison of model results transporting the odd nitrogen family with results transporting separate odd nitrogen species. *J. Geophys. Res.*, **94**, 9862–9872.

Fels, S. B., 1979: Simple strategies for inclusion of Voigt effects in infrared cooling rate calculations. *Appl. Optics*, **18**, 2634–2637.

——, and M. D. Schwarzkopf, 1975: The simplified exchange approximation: A new method for radiative transfer calculations. *J. Atmos. Sci.*, **32**, 1475–1488.

——, and ——, 1981: An efficient, accurate algorithm for calculating CO_2 15 μm band cooling rates. *J. Geophys. Res.*, **86**, 1205–1232.

Gallagher, C. C., C. A. Forsberg, A. S. Mason, B. W. Gandrud and M. Janghorbani, 1985: Total chlorine content in the lower stratosphere. *J. Geophys. Res.*, **90**, 10 747–10 752.

Garcia, R. R., and S. Solomon, 1983: A numerical model of the zonally averaged dynamical and chemical structure of the middle atmosphere. *J. Geophys. Res.*, **88**, 1379–1400.

——, and S. Solomon, 1985: The effect of breaking gravity waves on the dynamics and chemical composition of the mesosphere and lower thermosphere. *J. Geophys. Res.*, **90**, 3850–3868.

Geller, M. A., and M. F. Wu, 1987: Troposphere-stratosphere general circulation statistics. *Transport Processes in the Middle Atmosphere*, G. Visconti and R. R. Garcia, Eds., D. Reidel, 3–17.

Gille, J. C., J. M. Russell III, P. L. Bailey, E. G. Remsberg, L. L. Gordley, W. F. J. Evans, H. Fischer, B. W. Gandrud, A. Girard, J. E. Harries and S. A. Beck, 1984: Accuracy and Precision of the nitric acid concentrations determined by the limb infrared monitor of the stratosphere experiment on NIMBUS 7, *J. Geophys. Res.*, **89**, 5179–5190.

Goody, R. M., 1952: A statistical model for water vapor absorption. *Quart. J. Roy. Meteor. Soc.*, **78**, 165–169.

Guthrie, P. D., C. H. Jackman, J. R. Herman and C. J. McQuillan, 1984: A diabatic circulation experiment in a two-dimensional photochemical model. *J. Geophys. Res.*, **89**, 9589–9602.

Harwood, R. S., and J. A. Pyle, 1975: A two-dimensional mean circulation model for the atmosphere below 80 km. *Quart. J. Roy. Meteor. Soc.*, **101**, 723–747.

Haynes, P. H., and M. E. McIntyre, 1987: On the evolution of vorticity and potential vorticity in the presence of diabatic heating and frictional or other forces. *J. Atmos. Sci.*, **44**, 828–841.

Hitchman, M. H., and G. Brasseur, 1988: Rossby wave activity in a two-dimensional model: Closure for wave driving and meridional eddy diffusivity. *J. Geophys. Res.*, **93,** 9405–9417.

Jackman, C. H., R. S. Stolarski and J. A. Kaye, 1986: Two-dimensional monthly average ozone balance from Limb Infrared Monitor of the Stratosphere and Stratospheric and Mesospheric Sounder data. *J. Geophys. Res.*, **91,** 1103–1116.

——, ——, and ——, 1987: An intercomparison of nitrogen-containing species in Nimbus 7 LIMS and SAMS data. *J. Geophys. Res.*, **92,** 995–1008.

——, A. R. Douglass, P. D. Guthrie and R. S. Stolarski, 1989: The sensitivity of total ozone and ozone perturbation scenarios in a two-dimensional model due to dynamical inputs. *J. Geophys. Res.*, **94,** 9873–9887.

Jet Propulsion Laboratory, 1987: Chemical Kinetics and Photochemical Data for Use in Stratospheric Modeling. NASA Evaluation 8, JPL Publ. 87–41.

Jones, R. L., and J. A. Pyle, 1984: Observations of CH_4 and N_2O by the Nimbus 7 SAMS: A comparison with in-situ data and two-dimensional numerical model calculations. *J. Geophys. Res.*, **89,** 5263–5279.

Joseph, J. H., W. J. Wiscombe and J. A. Weinman, 1976: The delta-Eddington approximation for radiative flux transfer. *J. Atmos. Sci.*, **33,** 2452–2459.

Ko, M. K. W., N. D. Sze, M. Livshits, M. B. McElroy and J. A. Pyle, 1984: The seasonal and latitudinal behavior of trace gases and O_3 as simulated by a two-dimensional model of the atmosphere. *J. Atmos. Sci.*, **41,** 2381–2408.

——, K. K. Tung, D. K. Weisenstein and N. D. Sze, 1985a: A zonal mean model of stratospheric tracer transport in isentropic coordinates: Numerical simulation for nitrous oxide and nitric acid. *J. Geophys. Res.*, **90,** 2313–2329.

——, D. K. Weisenstein, N. D. Sze and K. K. Tung, 1985b: Simulation of O_3 distribution using a two-dimensional zonal-mean model in isentropic coordinate. *Atmospheric Ozone,* C. S. Zerefos and A. Ghazi, Eds., D. Reidel, 19–23.

——, M. B. McElroy, D. K. Weisenstein and N. D. Sze, 1986: Lightning: A possible source of stratospheric odd nitrogen. *J. Geophys. Res.*, **91,** 5359–5404.

——, N. D. Sze and D. K. Weisenstein, 1989: The role of dynamical and chemical processes in determining the stratospheric concentration of ozone in one-dimensional and two-dimensional models. *J. Geophys. Res.*, **94,** 9889–9896.

Lacis, A. A., and J. E. Hansen, 1987: A parameterization for the absorption of solar radiation in the earth's atmosphere. *J. Atmos. Sci.*, **31,** 118–133.

Lindzen, R. S., 1981a: Turbulence and stress owing to gravity and tidal breakdown. *J. Geophys. Res.*, **86,** 9707–9714.

——, 1981b: Some remarks on cumulus parameterization, Report on NASA-GISS workshop: Clouds in climate modelling and satellite observational studies, p. 42.

Mahlman, J. D., D. G. Andrews, D. L. Hartman, T. Matsuno and B. G. Murgatroyd, 1984: Transport of trace constituents in the stratosphere. *Dynamics of the Middle Atmosphere,* J. R. Holton and T. Matsuno, Eds., Terra Scientific, 387–416.

Malkmus, W., 1967: Random Lorentz band model with exponential tailed S^{-1} line-intensity distribution. *J. Opt. Soc. Am.*, **57,** 323–329.

Manabe, S., and R. T. Wetherald, 1967: Thermal equilibrium of the atmosphere with a given distribution of relative humidity. *J. Atmos. Sci.*, **24,** 241–259.

Murgatroyd, R. J., and F. Singleton, 1961: Possible meridional circulations in the stratosphere and mesosphere. *Quart. J. Roy. Meteor. Soc.*, **87,** 125–135.

Newell, R. E., J. W. Kidson, D. G. Vincent and G. J. Boer, 1974: *The General Circulation of the Tropical Atmosphere and Interactions with Extratropical Latitudes, Vol. 2.* MIT Press, 370 pp.

Newman, P. A., M. R. Schoeberl and R. A. Plumb, 1986: Horizontal mixing coefficients for two-dimensional chemical models calculated from National Meteorological Center data. *J. Geophys. Res.*, **91,** 7919–7924.

Olaguer, E. P., H. Yang and K. K. Tung, 1990: A reexamination of the radiative balance of the stratosphere. *J. Atmos. Sci.*, submitted.

Oort, A. H., 1983: Global atmospheric circulation statistics, 1958–1973, NOAA Prof. paper 14, US Govt. Printing office, 180 pp.

Ou, S. S., and K. N. Liou, 1983: Parameterization of carbon dioxide 15 μm band absorption and emission. *J. Geophys. Res.*, **88,** 5203–5207.

Plumb, R. A., and J. D. Mahlman, 1987: The zonally averaged transport characteristics of the GFDL general circulation/transport model. *J. Atmos. Sci.*, **44,** 298–327.

——, and D. D. McConalogue, 1988: On the meridional structure of long-lived tropospheric constituents. *J. Geophys. Res.*, **93,** 15 897–15 913.

Prather, M. J., 1986: Numerical advection by conservation of second-order moments. *J. Geophys. Res.*, **91,** 6671–6681.

Ramanathan, V., 1976: Radiative transfer within the earth's troposphere and stratosphere: A simplified radiative-convective model. *J. Atmos. Sci.*, **33,** 1330–1346.

——, and P. Downey, 1986: A nonisothermal emissivity and absorptivity formulation for water vapor. *J. Geophys. Res.*, **91,** 8649–8666.

Remsberg, E. E., and J. M. Russell, III, 1987: The near global distributions of middle atmospheric H_2O and NO_2 measured by the NIMBUS 7 LIMS experiment. *Transport Processes in the Middle Atmosphere.* G. Visconti and R. R. Garcia, Eds., D. Reidel, pp. 87–102.

Roberts, R. E., J. E. A. Selby and L. M. Biberman, 1976: Infrared continuum absorption by atmospheric water vapor in the 8–12 micron window. *Appl. Optics,* **15,** 2085–2090.

Rodgers, C. D., 1967: The use of emissivity in atmospheric radiation calculations. *Quart. J. Roy. Meteor. Soc.*, **93,** 43–54.

——, and C. D. Walshaw, 1966: The computation of infrared cooling rate in planetary atmospheres. *Quart. J. Roy. Meteor. Soc.*, **92,** 67–92.

——, and A. P. Williams, 1974: Integrated absorption of a spectral line with the Voigt profile. *J. Quant. Spectrosc. Radiat. Transfer,* **14,** 319–323.

Rosenfield, J. E., 1990: A simple parameterization of ozone infrared absorption for atmospheric heating rate calculations. *J. Geophys. Res.,*

Rothman, L. S., R. R. Gamache, L. R. Brown, R. A. Toth, H. M. Pickett, R. L. Poynter, J. M. Flaud, C. Camy-Peyrey, A. Barbe, N. Husson, C. P. Rinsland and M. A. H. Smith, 1987: The HITRAN database. *Appl. Optics,* **26,** 4058–4096.

Russel III, J. M., J. C. Gille, E. E. Remsberg, L. L. Gordley, P. L. Bailey, S. R. Drayson, J. Fischer, A. Girard, J. E. Harries and W. F. J. Evans, 1984: Validation of nitrogen dioxide results measured by the Limb Infrared Monitor of Stratosphere (LIMS) experiment on NIMBUS 7, *J. Geophys. Res.*, **89,** 5099–5107.

——, C. B. Farmer, C. P. Rinsland, R. Zander, L. Froidevaux, G. C. Toon, B. Gao, J. Shaw and M. Gunson, 1988: Measurements of odd nitrogen compounds in the stratosphere by the ATMOS experiment on spacelab 3. *J. Geophys. Res.*, **93,** 1718–1736.

Sasamori, T., J. London and D. V. Hoyt, 1972: Radiation budget of the Southern Hemisphere. *Meteorology of the Southern Hemisphere, Meteor. Monogr.,* Vol. 13, 9–23.

Schneider, H. R., and M. K. W. Ko, 1990: Response of an interactive two-dimensional model to ozone changes: An estimate of the radiative dynamical feedback effect. *J. Geophys. Res.*, **95,** 5657–5668.

——, ——, N. D. Sze, G-Y. Shi and W-C Wang, 1989: An evaluation of the role of eddy diffusion in stratospheric interactive two-dimensional models. *J. Atmos. Sci.*, **46,** 2079–2093.

Schutz, C., and W. L. Gates, 1972a: *Supplemental Global Climatic Data: January.* Rand Corp.

——, and ——, 1972b: *Global Climatic Data for Surface, 800 mb, 400 mb: July.* Rand Corp.

Sellers, W. D., *Physical Climatology.* University of Chicago Press, 272 pp.

Shia, R. L., Y. L. Yung, M. Allen, R. W. Zurek and D. Crisp, 1989: Sensitivity study of advection and diffusion coefficients in a two-dimensional stratospheric model using excess carbon 14 data. *J. Geophys. Res.*, **94,** 18 467–18 484.

——, Y. L. Ha, J.-S. Wen and Y. L. Yung, 1990: Two-dimensional atmospheric transport and chemistry model: Numerical experiments with a new advection algorithm. *J. Geophys. Res.*, **95,** 7467–7483.

Solomon, S., and R. R. Garcia, 1984: On the distribution of long-lived tracers and chlorine species in the middle atmosphere. *J. Geophys. Res.*, **89,** 11 633–11 644.

——, J. T. Kiehl, R. R. Garcia and W. Grose, 1986: Tracer transport by the diabatic circulation deduced from satellite observations. *J. Atmos. Sci.*, **43,** 1603–1617.

Somerville, R. C. J., P. H. Stone, M. Halem, J. E. Hansen, J. S. Hogan, L. M. Druyan, G. Russell, A. A. Lacis, W. J. Quirk and J. Tenenbaum, 1974: The GISS model of the global atmosphere. *J. Atmos. Sci.*, **31,** 84–117.

Stordal, F., I. S. A. Isaksen and K. Horntveth, 1985: A diabatic circulation two-dimensional model with photochemistry: Simulations of ozone and ground released traces. *J. Geophys. Res.*, **90,** 5757–5776.

Tung, K. K., 1982: On the two-dimensional transport of stratospheric trace gases in isentropic coordinates. *J. Atmos. Sci.*, **39,** 2330–2355.

——, 1984: Modeling of tracer transport in the middle atmosphere. *Dynamics of the Middle Atmosphere,* J. R. Holton and T. Matsuno, Eds., Terra Scientific, 412–444.

Tung, K. K., 1986: Nongeostrophic theory of zonally averaged circulation. Part I: Formulation. *J. Atmos. Sci.*, **43,** 2600–2618.

——, 1987: A coupled model of zonally averaged dynamics, radiation and chemistry. *Transport Processes in the Middle Atmosphere,* G. Visconti and R. R. Garcia, Eds., D. Reidel, pp. 183–198.

——, and H. Yang, 1988: Dynamical component of seasonal and year-to-year changes in Antarctic and global ozone. *J. Geophys. Res.*, **93,** 12 537–12 559.

World Meteorological Organization, 1986: Atmospheric Ozone 1985: Assessment of our understanding of processes controlling its present distribution and change. WMO Rep. 16, Global Ozone Res. and Monit. Proj., Geneva.

Yang, H., K. K. Tung and E. P. Olaguer, 1989: Two-dimensional model simulation of ozone climatology and year-to-year variations. *Ozone in the Atmosphere: Proc. of the Quadrennial Ozone Symposium 1988 and Troposphere Ozone Workshop,* Göttingen, Germany (FRG), 613–616.

——, —— and ——, 1990: Nongeostrophic theory of zonally averaged circulation, Part II: Eliassen-Palm flux divergence and isentropic mixing coefficient. *J. Atmos. Sci.*, **47,** 215–241.